Available online at www.sciencedirect.com
SCIENCE DIRECT
Geochimica et Cosmochimica Acta 70 (2006) 3040–3058
Geochimica
www.elsevier.com/locate/gca

In situ SHRIMP U–Pb dating of monazite integrated with petrology and textures: Does bulk composition control whether monazite forms in low-Ca pelitic rocks during amphibolite facies metamorphism?

Birger Rasmussen [a,*], Janet R. Muhling [b], Ian R. Fletcher [a], Michael T.D. Wingate [c]

[a] School of Earth and Geographical Sciences, The University of Western Australia, 35 Stirling Highway, Crawley, WA 6009, Australia
[b] Centre for Microscopy and Microanalysis, The University of Western Australia, 35 Stirling Highway, Crawley, WA 6009, Australia
[c] Tectonics Special Research Centre, School of Earth and Geographical Sciences, The University of Western Australia, 35 Stirling Highway, Crawley, WA 6009, Australia

Received 11 November 2005; accepted in revised form 20 March 2006

Abstract

Bulk composition and specific reaction history among common silicate minerals have been proposed as controls on monazite growth in metapelitic rocks during amphibolite facies metamorphism. It has also been implied that monazite that formed during greenschist facies metamorphism may be preserved unchanged under upper amphibolite facies conditions. If correct, this would make the interpretation of monazite ages in polymetamorphic rocks exceedingly difficult, because isotopic dates could vary significantly in rocks that have experienced identical metamorphic conditions but differ only slightly in whole-rock composition. Low-Ca pelitic schists from the Mount Barren Group in southwestern Australia display a range of whole-rock compositions in AFM space and different peak mineral assemblages resulting from amphibolite facies metamorphism (~8 kb, 650 °C). In this study, we test whether bulk composition controls the formation of monazite through geochronology and textural evidence linking monazite growth with deformation and peak metamorphism. X-ray element mapping of monazite from the metapelitic rocks reveals concentric zoning in many grains with compositionally distinct cores and rims. In situ SHRIMP U–Pb geochronology of monazite yields two $^{207}Pb/^{206}Pb$ age populations. The cores, and texturally early monazite, give an age of 1209 ± 10 Ma, interpreted to record prograde metamorphism, whereas the rims and "late" monazite define a single population of 1186 ± 6 Ma, which is considered the likely age of peak thermal metamorphism. The growth of monazite was widespread in low-Ca pelitic schists representing a broad range of compositions in AFM space, indicating that variations in bulk composition in AFM space did not control the formation of monazite during amphibolite facies metamorphism in the Mount Barren Group.

1. Introduction

Monazite ([LREE,Ca,Th]PO_4) is a common accessory mineral in many igneous and metamorphic rocks (Overstreet, 1967; Chang et al., 1998; Bea and Montero, 1999; Spear and Pyle, 2002). It is an important mineral for U–Pb geochronology (Parrish, 1990; Montel et al., 1996; Harrison et al., 2002) and has been mostly used to date amphibolite and granulite facies metamorphism (Bingen and van Breemen, 1998; Zhu and O'Nions, 1999; Hawkins and Bowring, 1999; Stern and Berman, 2000; Rubatto et al., 2001). Monazite is only considered to become abundant during amphibolite facies metamorphism, at temperatures corresponding with the staurolite isograd (Smith and Barreiro, 1990; Kingsbury et al., 1993). Its formation is commonly linked to the breakdown of other accessory phases, particularly allanite (LREE, Ca, Al silicate), during prograde metamorphism (Overstreet, 1967; Ferry, 2000; Wing et al., 2003). However, it has recently been suggested

* Corresponding author. Fax: +61 8 6488 1037.
E-mail address: brasmuss@cyllene.uwa.edu.au (B. Rasmussen).

0016-7037/$ - see front matter © 2006 Elsevier Inc. All rights reserved.
doi:10.1016/j.gca.2006.03.025

that accessory minerals are not necessarily required to form monazite, but rather, that reactions among common metamorphic silicate minerals may control the growth and dissolution of monazite at various grades (Pyle and Spear, 2003; Kohn and Malloy, 2004). In particular, monazite growth has been linked to garnet destruction and staurolite formation via the reaction (garnet + chlorite + muscovite = biotite + plagioclase + staurolite + H_2O) (Kohn and Malloy, 2004). During this reaction, monazite is interpreted to form from P liberated from garnet and light REE released from the sheet silicates (Kohn and Malloy, 2004).

Similarly, reaction among common silicate minerals has been used to explain polymodal monazite age distributions in low-Ca metapelitic rocks from the Mount Barren Group in southwestern Australia (Fig. 1) (Fitzsimons et al., 2005). It was argued that a similar reaction involving garnet destruction (garnet + chlorite + muscovite = staurolite + biotite + quartz + H_2O) was solely responsible for the growth of monazite during peak amphibolite facies metamorphism, while monazite grains recording older ages are relicts of an earlier greenschist facies event (Fitzsimons et al., 2005).

Furthermore, it was proposed that this reaction only occurred in schists with a specific bulk composition represented by the phase assemblage Grt-St-Bt-Ms-Qtz (assemblage 2; Table 1; major phase abbreviations after Kretz, 1983). Schists containing garnet but no staurolite were considered too Fe-rich to undergo the inferred monazite-forming reaction, whereas samples containing staurolite, but no garnet (assemblage 3) or kyanite (assemblages 4–6) were considered too Mg- and/or Al-rich to have undergone the reaction. If correct, this hypothesis would have major implications for monazite geochronology, implying that the timing of monazite growth can vary significantly with subtle differences in bulk composition and that monazite that formed during low-grade metamorphism can survive unmodified during upper amphibolite facies metamorphism. This would create large uncertainties in the interpretation of monazite age data, particularly for rocks that underwent multiple metamorphic events.

Table 1
Mineral assemblages in amphibolite facies schists and micaceous quartzites at Barrens Beach, East Mount Barren and West Beach

Assemblage no.	Peak metamorphic assemblage	Mon	Xt
1	Grt-Bt-Ms-Qtz	Present	Present
2	Grt-St-Bt-Ms-Qtz	Present	n.o.[a]
3	St-Bt-Ms-Qtz	Present	Present
4	St-Bt-Ky-Ms-Qtz	Present	Present
5	Bt-Ky-Ms-Qtz	Present	Present
6	Grt-St-Bt-Ky-Ms-Qtz	Present	Present
7	Grt-Bt-Ky-Qtz	n.e.[b]	n.e.
8	Bt-Ky-Qtz	n.e.	n.e.
9	Ky-Ms-Qtz	Present	Present

[a] n.o., not observed.
[b] n.e., not examined.

In this paper, we present new petrographic, geochemical and geochronological data for monazite in amphibolite facies low-Ca metapelitic rocks with a wide range of phase assemblages from the same locality as that described by Fitzsimons et al. (2005), the Mount Barren Group in the Albany–Fraser Orogen, southwestern Australia (Fig. 1). The objectives are to: (i) establish the timing of amphibolite

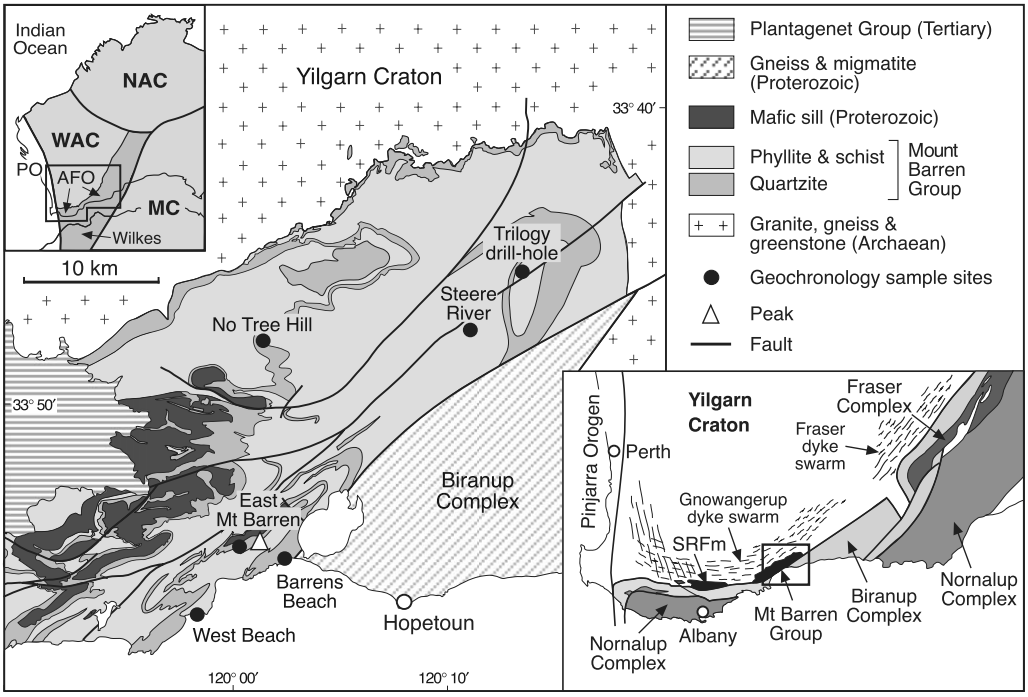

Fig. 1. Map showing the regional geology of the Albany–Fraser Orogen, southwestern Australia and the location of sample sites in the Mount Barren Group. MC, Mawson Craton; NAC, North Australian Craton; WAC, West Australian Craton; AFO, Albany–Fraser Orogen; PO, Pinjarra Orogen; SRFm, Stirling Range Formation.

facies metamorphism, allowing previous age estimates for this event, which vary by ~170 million years, to be evaluated, and (ii) test the proposal that bulk composition and reaction history among silicate phases controls whether monazite will form during amphibolite facies metamorphism of low-Ca pelitic schists.

2. Geological setting

2.1. Albany–Fraser Orogen

The Albany–Fraser Orogen in southwestern Australia is an arcuate Mesoproterozoic orogenic belt that comprises the E-W trending Albany Mobile Belt and the NE-SW trending Fraser Mobile Belt. The orogen has been divided into: (1) a bordering autochthonous northern domain containing structurally and thermally reworked mid- to late Archaean granites of the southern margin of the Yilgarn Craton (Fletcher et al., 1983; Beeson et al., 1988; Myers, 1990; Black et al., 1992), and (2) the allochthonous Biranup, Fraser and Nornalup Complexes, which mostly comprise granulite facies orthogneis and less abundant paragneiss, metagabbro, and late-tectonic granites (Condie and Myers, 1999). A series of low- to medium-grade metasedimentary successions, including the Mount Barren Group and Stirling Range Formation, crop out along the boundary between the southern Yilgarn Craton and the Albany–Fraser Orogen (Fig. 1).

Most workers have recognized two discrete thermotectonic episodes in the Albany–Fraser Orogen (Beeson et al., 1988; Fletcher et al., 1991; Black et al., 1992; Nelson et al., 1995; Clark et al., 1999, 2000; Bodorkos and Clark, 2004). Clark et al. (2000) placed the first event (Stage I) between ~1345 Ma and ~1260 Ma, with 45 m.y. of quiescence prior to Stage II between ~1214 Ma and ~1140 Ma. Stage I involved high-grade metamorphism, thrusting, transpression and felsic plutonism and has been interpreted to record continental collision and suturing of the West Australian Craton and the Mawson Craton (comprising southern Australia and Antarctica; Clark et al., 2000). Stage II coincided with the emplacement of ~1210 Ma dyke swarms along the craton margin and within the Albany–Fraser Orogen (Evans, 1999; Wingate et al., 2000, 2005; Rasmussen and Fletcher, 2004). Stage II involved widespread metamorphism (1215–1180 Ma) ranging from greenschist-amphibolite facies (Rasmussen et al., 2002; Dawson et al., 2003) to granulite facies (Clark et al., 2000; Bodorkos and Clark, 2004), extensive deformation and the intrusion of late- to post-tectonic granites. This stage of tectonism has been linked to intracratonic reactivation (Clark et al., 2000). A similar tectonic history is recorded (~1340 to ~1150 Ma) in rocks from the Wilkes Province of East Antarctica (Post et al., 1997; Fitzsimons, 2003), with which the Albany–Fraser Orogen has been correlated (Black et al., 1992; Sheraton et al., 1995; Clark et al., 2000).

By contrast, others have proposed that peak metamorphism in the Mount Barren Group occurred at ~1030 Ma, rather than at ~1200 Ma, based on SHRIMP analysis of multi-aged monazite separated from a garnet-staurolite metapelite (Wetherley et al., 1998; Fitzsimons et al., 2005). Based on this interpretation, Fitzsimons and Buchan (2005) and Fitzsimons and Kinny (2005) proposed a third stage of tectonism (Stage III) in the Albany–Fraser Orogen at ~1030 Ma. Stage III involved amphibolite facies metamorphism and northwest-directed contraction, consistent with a period of crustal thickening (Fitzsimons and Buchan, 2005), and was synchronous with the last stage of a thermotectonic event preserved in the Pinjarra Orogen to the west. The absence of 1030 Ma dates in previous geochronological studies of pelitic schists from the same locality (e.g., Dawson, 2000; Dawson et al., 2003) was attributed to the formation of monazite during peak metamorphism by a specific reaction among silicate minerals in a very restricted bulk composition (Fitzsimons et al., 2004, 2005). The lack of 1030 Ma dates in the rest of the Albany–Fraser Orogen, was explained by the recrystallization and dehydration of basement rocks at high metamorphic grades during Stages I and II (Fitzsimons and Buchan, 2005). The interpretation of polymodal monazite dates from the Mount Barren Group therefore has ramifications for the use of monazite to date high-grade metamorphic events and for the tectonic reconstruction of the Rodinia supercontinent.

2.2. Mount Barren Group

The Mount Barren Group is a Proterozoic metasedimentary succession comprising mainly quartzite, phyllite and schist, with minor conglomerate and dolomite, intruded by a thick mafic sill (Sofoulis, 1958; Thom et al., 1977; Thom and Chin, 1984; Witt, 1997, 1998; Wetherley, 1998). In situ SHRIMP U–Pb geochronology of diagenetic xenotime in phosphatic sandstone from the Trilogy drillhole (Fig. 1) suggests that the succession is older than 1696 ± 7 Ma (Vallini et al., 2002), whereas detrital zircon grains in quartzites from Barrens Beach, No Tree Hill and Steere River (Fig. 1) indicate a maximum age of ~1790 Ma (Nelson et al., 1995; Nelson, 1996, 2001; Dawson et al., 2002).

The succession experienced lower greenschist ($T < 350$ °C) to mid-upper amphibolite facies metamorphism (~8 kbars and 650 °C). Metamorphic isograds have not been mapped, but low-grade sericite-chlorite assemblages are found in the north and west, while the grade increases to the south and east (Witt, 1997), with the highest grade rocks exposed along the coast. Uplift of the high-grade rocks probably occurred across a series of NE-SW trending faults late in the evolution of the Albany–Fraser Orogen. Multiple phases of deformation have been identified in the Mount Barren Group (Thom and Chin, 1984; Witt, 1997; Wetherley, 1998). Five phases of folding were mapped by Wetherley (1998): F_1–F_4 structures were inter-

preted to represent stages in a single tectonic event with peak metamorphism occurring during or shortly after F_4 (Hollingsworth, 1996; Stephens, 1996; Dawson, 2000; Dawson et al., 2003; Fitzsimons et al., 2005). F_5 structures were related to a second deformational event linked to a phase of retrogression at shallow crustal levels, and comprise upright kinks (F_5) and a weak crenulation cleavage.

Two dominant fabrics were recognized by Wetherley (1998); (S_2 and S_4, notation used in this paper) and others (Thom, 1977; Hollingsworth, 1996; Witt, 1997, 1998; Stephens, 1996; Dawson, 2000; Dawson et al., 2003), which have been correlated across the Mount Barren Group (Wetherley, 1998). The fabrics are axial planar foliations associated with isoclinal folds that are attributed to early N-S and later NW-SE compression (Wetherley, 1998). They are consistent with the overall trend of structures elsewhere in the Albany–Fraser Orogen, and point to simultaneous metamorphism and deformation within the ~1345 Ma to ~1140 Ma span of the orogen.

2.3. Metamorphic mineral assemblages and bulk composition

A wide range of metamorphic assemblages has been documented in amphibolite facies metapelitic rocks from three localities in the Mount Barren Group: Barrens Beach, West Beach and East Mount Barren (Table 1 and Fig. 2; assemblages 1–9). All assemblages occur in Ca-poor rocks (<0.5 wt% CaO) and phase relationships can be represented in AFM projections (Fig. 2). Assemblages 1–5, comprising garnet-biotite (1), garnet-staurolite-biotite (2), staurolite-biotite (3), staurolite-biotite-kyanite (4) and biotite-kyanite (5), all with quartz and muscovite in excess, reflect a trend of increasing Mg and/or Al (Fig. 2). Assemblage 6 comprises garnet-biotite-staurolite-kyanite with excess muscovite and quartz. Assemblages 7 (Grt-Bt-Ky-Qtz) and 8 (Bt-Ky-Qtz) are devoid of muscovite and are not considered further, because they cannot be portrayed on the phase diagrams used to interpret the other muscovite-bearing assemblages. Assemblage 9 (Ms-Ky-Qtz) was identified in this study from East Mount Barren and is the most aluminous of all the samples. All the assemblages are interpreted to have experienced the same metamorphic conditions and to have stabilized at peak P and T of ~8 kbar and 650 °C (Fig. 3; Wetherley, 1998; Fitzsimons et al., 2005). The variations in whole-rock Al, Fe and Mg contents (Fig. 2c) are considered to reflect differences in the compositions of the pre-metamorphic sedimentary rocks (Hollingsworth, 1996; Wetherley, 1998; Fitzsimons et al., 2005).

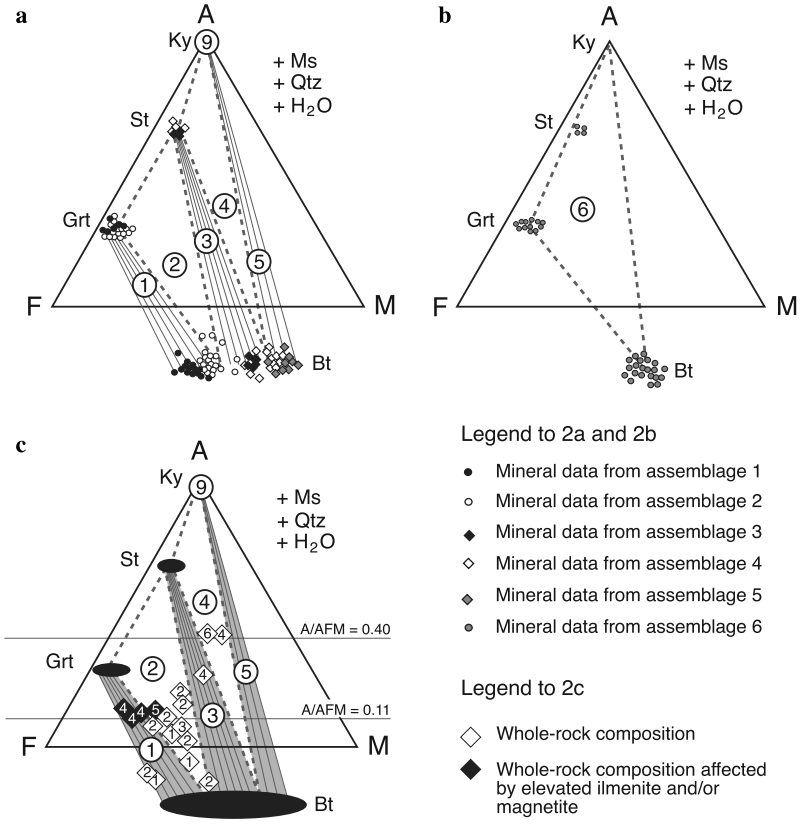

Fig. 2. (a) and (b) Mineral chemical data for metasedimentary rocks from the Mount Barren Group plotted on an AFM projection from muscovite, quartz and H_2O (after Fitzsimons et al., 2005). Assemblages 1–6, and 9 are interpreted to have stabilized at a single P and T, with different mineral stabilities reflecting bulk-rock chemical variations that cannot be depicted in this projection. (c) Whole-rock geochemical data from Hollingsworth (1996) and Wetherley (1998) plotted with the mineral stability fields from (a) showing the influence of variations in bulk rock Fe, Mg and Al on mineral assemblages.

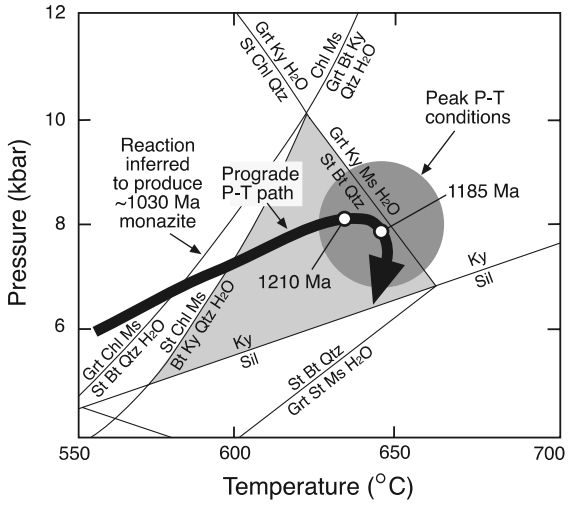

Fig. 3. Petrogenetic grid constructed by Wetherley (1998) for the KFMASH system showing peak *P–T* conditions and inferred *P–T* path for metapelitic rocks from the Mount Barren Group.

The relationship between deformation and metamorphism in the Mount Barren Group has been described in previous studies (Hollingsworth, 1996; Stephens, 1996; Witt, 1997, 1998; Wetherley, 1998; Dawson, 2000; Dawson et al., 2003). The earlier of the two main foliations (S_2) is typically defined by parallel crystals of quartz, muscovite, ilmenite/magnetite and biotite, and is locally crenulated by S_4. The S_4 foliation is defined by aligned crystals of quartz, muscovite, biotite, ilmenite/magnetite, and in places, tourmaline and apatite. The S_4 foliation is overprinted by coarse kyanite, staurolite, biotite and muscovite porphyroblasts (Fig. 4a and c), although in places, the S_4 fabric wraps around kyanite, muscovite, biotite, staurolite, garnet and magnetite (Fig. 4b), suggesting that most porphyroblasts (except garnet and magnetite) grew syn- to post S_4. In most cases, there is no evidence for resorption of garnet or staurolite along their mutual grain boundaries (Fig. 4d). Garnet is commonly subidioblastic and is included or partly included within larger staurolite porphyroblasts (Fig. 4d). Garnet crystals may contain an inclusion-rich core (referred to as Grt-1 by Fitzsimons et al., 2005) that preserves an earlier fabric (S_2), which may be surrounded by a relatively inclusion-free rim (Grt-2). Grt-2 has been interpreted as a later stage of garnet growth that locally overprints S_4, and is related to the prograde destruction of staurolite and biotite (Fitzsimons et al., 2005). Biotite crystals in assemblages

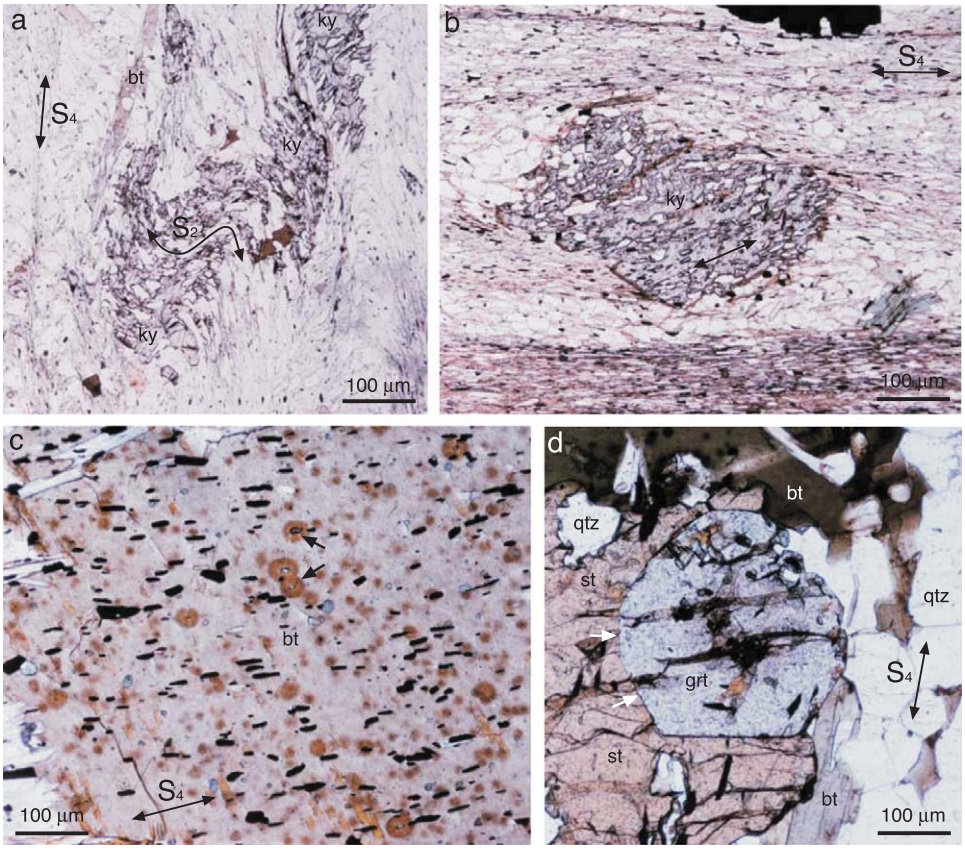

Fig. 4. Optical photomicrographs showing (a) single, inclusion-rich kyanite (ky) porphyroblast that overprints the S_2 and S_4 foliation defined by muscovite (ms) and quartz (qtz); (b) single, inclusion-rich kyanite (ky) porphyroblast that is wrapped by the S_4 foliation, with asymmetric, quartz-rich pressure shadows; (c) Coarse biotite that overprints the S_4 fabric containing ilmenite (black) and mostly monazite, surrounded by pleochroic radiation haloes, aligned with the S_4 fabric; (d) Idioblastic garnet embedded in a staurolite porphyroblast. Note the sharp planar boundaries between the garnet and staurolite.

1–6, including grains aligned with, and overprinting, S_4, contain abundant pleochroic haloes (Fig. 4c) produced by zircon, monazite, xenotime and rutile inclusions. Sillimanite occurs in several samples, where it overprints the S_4 foliation and may have formed during uplift and decompression. Chlorite is present in some samples as an alteration product of biotite and garnet.

2.4. Isotopic constraints on the timing of metamorphism

2.4.1. Rb–Sr isochron data

Rb–Sr whole-rock and mineral analyses on five samples (Ky-Bt-Ms-Qtz schists) from Barrens Beach gave a scattered isochron trend corresponding to an age of 1077 ± 22 Ma, but with MSWD = 27.6 (Thom et al., 1981). The date was considered to represent the age of the final episode of folding (equivalent to F_4). Eight samples (Qtz-Bt-Ms-St; Qtz-Bt-Ms-St-Ky and Qtz-Bt-Ms-Grt schists) from West Beach yielded imprecise and scattered data that failed to give an isochron.

2.4.2. Pb/Pb isochron data

Garnet porphyroblasts were separated from two samples: a garnet-biotite-muscovite-quartz schist (sample 9305/039 from East Mount Barren) and a garnet-staurolite-biotite-muscovite-quartz schist (sample WBCH1 from West Beach), whereas staurolite porphyroblasts were only separated from WBCH1 (Wetherley, 1998). Sequential leaching of garnet from sample 9305/039 produced a Pb/Pb isochron trend of 1220 ± 26 Ma (MSWD = 0.67; $n = 5$). Leaches of garnet from WBCH1 yielded a 10-point isochron trend of 1119 ± 66 Ma (MSWD = 26.3), whereas staurolite leaches gave 1224 ± 13 Ma (MSWD = 7.8). Only the garnet from sample 9305/039 was considered to define an isochron and the date was interpreted to record the age of garnet growth and the timing of the main phase of deformation and amphibolite-facies metamorphism (Wetherley and McNaughton, 1995).

2.4.3. SHRIMP U–Pb data for monazite in garnet separates

Monazite was separated from the garnet concentrates of sample WBCH1 (Wetherley, 1998). Sixteen SHRIMP analyses were conducted on 12 monazite grains, giving a spread of $^{207}Pb/^{206}Pb$ dates that range from 1042 ± 6 Ma to 936 ± 15 Ma (1σ) and show a strong correlation with Th content. An age of 1028 ± 7 Ma was cited for the oldest population by Wetherley (1998), whereas Fitzsimons et al. (2005), using the same data, derived an age of 1027 ± 8 Ma for the oldest nine grains. This date was interpreted as the age of prograde or peak amphibolite facies metamorphism. However, these dates do not conform to a single age population, having MSWD = 2.5. A cluster of younger dates gave a $^{207}Pb/^{206}Pb$ age of 943 ± 19 Ma (MSWD = 0.4; $n = 3$), which may be related to a low-temperature retrograde event (D_5) (Fitzsimons et al., 2005).

2.4.4. In situ SHRIMP U–Pb data for monazite and xenotime

Monazite and xenotime from pelitic schists and micaceous quartzites from the Mount Barren Group were described by Dawson et al. (2003) (Table 2). In situ U–Pb SHRIMP analyses were carried out on ten monazite crystals from Barrens Beach and East Mount Barren, producing a weighted mean $^{207}Pb/^{206}Pb$ age of 1194 ± 8 Ma (MSWD = 3.5; $n = 15$). The analyzed monazite grains occur as inclusions within coarse muscovite, staurolite and biotite crystals, and in the matrix as idioblastic crystals aligned with the dominant S_4 fabric. The high MSWD was interpreted to reflect mixing of two or more populations.

In situ SHRIMP analysis of xenotime in pelitic schists from Barrens Beach yielded a weighted mean $^{207}Pb/^{206}Pb$ age of 1206 ± 8 Ma (MSWD = 0.73; $n = 14$). The dated grains occur in the matrix and as inclusions within coarse overprinting biotite and kyanite porphyroblasts. Based on textural relationships, Dawson et al. (2003) interpreted an age of 1205 ± 10 Ma as the likely timing of peak metamorphism in the Mount Barren Group.

2.5. Interpretation of isotopic data by Fitzsimons et al. (2005)

Fitzsimons et al. (2005) argued that ~1030 Ma monazite records the age of prograde metamorphism or peak amphibolite facies metamorphism in the Mount Barren Group. The conclusions of Dawson (2000) and Dawson et al. (2003) were rejected on the premise that the dated monazite and xenotime grains are relicts of an earlier metamorphic assemblage included within the peak metamorphic minerals. The formation of ~1200 Ma monazite and xenotime was attributed to a greenschist facies event that predated amphibolite facies metamorphism by 170 million years (Fitzsimons et al., 2005).

The ~1200 Ma Pb/Pb isochron dates obtained from garnet (sample 9305/039; assemblage 1) and staurolite (sample WBCH1; assemblage 2) were interpreted to reflect the age of ~1200 Ma monazite inclusions, rather than the age of the garnet or staurolite. Garnet from WBCH1, which gives a 10-point errorchron age of 1119 ± 66 Ma (MSWD = 26.3), was interpreted to record the presence of both ~1200 Ma and ~1030 Ma monazite inclusions in equal proportions.

The presence of ~1200 Ma monazite and absence of 1030–950 Ma monazite in samples of assemblages 3–6 dated by Dawson et al. (2003) was attributed to differences in bulk composition (Fitzsimons et al., 2005). WBCH1, which was the only sample to yield 1030–950 Ma monazite, was also the only pelitic schist with the appropriate bulk composition to have undergone garnet breakdown and staurolite growth (and peak metamorphic monazite growth) by the reaction:

Table 2
Summary of geochronology from the Mount Barren Group

Sample ID	Peak mineral assemblage	Ass. no.[a]	Grt date (Ma)	St date (Ma)	Mon date (Ma)	Xt date (Ma)
West Beach and East Mount Barren (Wetherley, 1998)						
9305/039	Qtz-Grt-Bt-Ms-[St][b]	1&2[b]	1220 ± 26	n.a.[c]	n.a.	n.o.[d]
WBCH1[e]	Qtz-Grt-St-Bt-Ms[f]	2[f]	1119 ± 66	1224 ± 13	1027 ± 8	Unknown
WBCH1[e]	Qtz-Grt-St-Bt-Ms[f]	2[f]	1119 ± 66	1224 ± 13	943 ± 19	Unknown
Barrens Beach and West Beach (Dawson, 2000; Dawson et al., 2003)						
BB-01	Qtz-Ms-Bt-St-Ky	4	n.o.	n.a.	n.a.	n.a.
BB-02	Qtz-Ms-Bt-Ky-St	4	n.o.	n.a.	1194 ± 7[g]	n.a.
BB-03	Qtz-Bt-Ms-Ky-St	4	n.o.	n.a.	1194 ± 7	n.a.
BB-05	Qtz-Ms-Ky-Bt-St	4	n.o.	n.a.	n.a.	1206 ± 8[h]
BB-06	Qtz-Ms-Ky-Bt	5	n.o.	n.o.	n.a.	1206 ± 8
BB-09	Qtz-Bt-Ky-Ms-St	4	n.o.	n.a.	n.a.	1206 ± 8
BB-10	Qtz-Ms-Bt-St	3	n.o.	n.a.	n.a.	1206 ± 8
9306/011	Qtz-Ky-Bt-Ms-St	4	n.o.	n.a.	n.a.	n.a.
9305/025	Qtz-St-Bt-Grt-[Ky]-Ms	2&6	n.a.	n.a.	1194 ± 7	n.a.
West Beach and East Mount Barren (this study)						
WB-01	Qtz-Bt-Ms-Ky	5	n.o.	n.o.	1211 ± 13 (cores)	n.a.
WB-01	Qtz-Bt-Ms-Ky	5	n.o.	n.o.	1187 ± 10 (rims)	n.a.
WB-04	Qtz-Ms-Bt-Grt	1	n.o.	n.o.	1196 ± 6 (undif.)	n.a.
9305/039	Qtz-Bt-Ms-Grt-[St]	1&2	n.a.	n.o.	1202 ± 8 (undif.)	n.a.
EMB-01	Qtz-Ms-Ky	9	n.a.	n.a.	1185 ± 8	n.a.
9306/011	Qtz-Ms-Ky-St-Bt	4	n.o.	n.a.	~1205	n.a.
9306/011	Qtz-Ms-Ky-St-Bt	4	n.o.	n.a.	~1193	n.a.

[a] Peak mineral assemblage numbers from Table 1.
[b] The mineralogy of some hand-specimens is heterogeneous on the cm-scale and comprises two or more peak mineral assemblages.
[c] n.a., not analysed.
[d] n.o., not observed.
[e] The locality details of this sample are unknown, but it is thought to come from West Beach.
[f] Apart from the presence of garnet and staurolite, the mineralogy and chemical composition of this sample is unknown (no material remains and a thin section was never made).
[g] Date is based on 12 in situ SHRIMP analyses of monazite grains from peak mineral assemblages 4 and 6.
[h] Date is based on 14 in situ SHRIMP analyses of xenotime grains from peak mineral assemblages 3–5.

$$\text{garnet} + \text{chlorite} + \text{muscovite} = \text{staurolite} + \text{biotite} + \text{quartz} + H_2O$$

All other bulk compositions were either too Fe-rich (assemblage 1) or Mg- and Al-rich (assemblages 3–6) to have undergone this reaction (Fitzsimons et al., 2005). Instead, these rocks were considered to preserve monazite and xenotime that grew during an earlier (~1200 Ma) greenschist facies event.

3. Samples and analytical methods

3.1. Sample details

Thirty-five polished thin sections were made from samples collected from West Beach as well as material archived by Wetherley (1998) and Dawson (2000) from West Beach, Barrens Beach and East Mount Barren. Twenty polished thin sections from previous studies (Wetherley, 1998; Dawson, 2000) were also studied. Samples from all three localities include specimens from each of the main peak metamorphic assemblages (assemblages 1–6 and 9; Table 1), which represent a broad range of bulk compositions in AFM space (Fig. 2). Samples were investigated by optical microscope and a Jeol JSM 6400 scanning electron microscope (SEM) equipped with an Oxford LINK energy dispersive spectrometer (EDS) located in the Centre for Microscopy and Microanalysis (CMM) at the University of Western Australia (UWA).

3.2. Electron microprobe element mapping

X-ray element maps were collected from monazite crystals in eight metapelite samples. The maps were collected and processed using an automated Jeol JSM6400 SEM fitted with three wavelength dispersive crystal spectrometers housed in the CMM at UWA, and Moran Scientific software. Operating conditions were 20 kV accelerating voltage, 100 nA beam current and a spot size of 3–5 μm. Synthetic phosphates and glasses, and natural minerals were used as standards. Pixel sizes of the maps varied according to the size of the crystal mapped, from 0.17 μm to 1.14 μm. Counting times were 50 ms per pixel.

3.3. SHRIMP U–Pb geochronology

Areas containing coarse monazite crystals (>15 μm) were drilled or cut from polished thin sections and cast in 25 mm epoxy discs, referred to as "mounts". The sample

Table 3
Summary of in situ SHRIMP U–Pb age data for monazite from the Mount Barren Group

Analysis spot[a]	U (ppm)	Th (%)	Th/U	f206[b] (%)	$^{207}Pb^*/^{206}Pb^*$[c]	±	$^{206}Pb^*/^{238}U$	±	$^{207}Pb^*/^{235}U$	±	$^{208}Pb^*/^{232}Th$	±	Conc.[d] (%)	$^{207}Pb^*/^{206}Pb^*$[e] Age (Ma)	± (Ma)
Sample WB-01 (Ky-Bt-Ms-Qtz schist; assemblage 5)															
Cores (*zones 1 to 3*)															
04122A.6-1	4804	8.2	17.0	0.121	0.0807	0.0006	0.2174	0.0042	2.419	0.051	0.0650	0.0012	104	1215	14
04122A.9.1	5882	1.1	1.9	0.104	0.0813	0.0004	0.2127	0.0039	2.386	0.047	0.0636	0.0014	101	1230	10
04122C.1-2	3083	3.3	10.6	0.260	0.0812	0.0006	0.2112	0.0040	2.364	0.051	0.0617	0.0012	101	1225	15
04122D.1-1	3701	0.6	1.5	0.274	0.0804	0.0006	0.2088	0.0041	2.316	0.050	0.0600	0.0014	101	1208	14
04122D.2-1	3217	6.6	20.6	0.244	0.0795	0.0006	0.2018	0.0039	2.213	0.048	0.0606	0.0011	100	1186	14
04122D.2-2	2807	0.4	1.4	0.157	0.0803	0.0006	0.2046	0.0041	2.264	0.050	0.0633	0.0014	100	1203	14
04122D.3-2	4284	1.4	3.2	0.186	0.0804	0.0004	0.2008	0.0037	2.225	0.043	0.0617	0.0011	98	1206	9
04122E.6-2	2757	0.7	2.5	0.380	0.0800	0.0006	0.2072	0.0038	2.286	0.047	0.0626	0.0011	101	1197	14
04122F.1-2	3247	1.6	5.0	0.228	0.0809	0.0006	0.2005	0.0038	2.236	0.047	0.0625	0.0011	97	1219	15
Rims (*zone 4*)															
04122A.1-2	2825	3.7	12.9	0.200	0.0798	0.0006	0.2039	0.0038	2.243	0.047	0.0634	0.0011	100	1192	14
04122A.6-2	2342	2.9	12.4	0.288	0.0795	0.0009	0.2106	0.0044	2.308	0.057	0.0631	0.0012	104	1184	22
04122A.9-2	3255	4.1	12.7	0.100	0.0802	0.0005	0.2072	0.0039	2.289	0.048	0.0624	0.0011	101	1201	13
04122B.1-2	2861	4.4	15.4	0.144	0.0796	0.0006	0.2032	0.0038	2.231	0.047	0.0607	0.0011	100	1188	14
04122B.5-2	2930	4.8	16.5	0.096	0.0790	0.0005	0.1991	0.0038	2.169	0.045	0.0604	0.0011	100	1172	12
04122C.1-1	3695	5.6	15.1	0.095	0.0795	0.0005	0.2055	0.0040	2.253	0.048	0.0602	0.0011	102	1184	12
04122C.4-2	3026	5.0	16.5	0.095	0.0794	0.0005	0.2013	0.0038	2.204	0.045	0.0614	0.0011	100	1182	12
04122D.1-2	4370	5.6	12.9	0.163	0.0797	0.0005	0.2025	0.0039	2.225	0.046	0.0615	0.0011	100	1190	12
04122D.2-3	3009	3.9	12.8	0.095	0.0797	0.0004	0.1974	0.0037	2.170	0.043	0.0607	0.0011	98	1190	10
04122E.6-1	2254	3.6	15.9	0.107	0.0791	0.0005	0.1998	0.0038	2.180	0.044	0.0605	0.0011	100	1176	12
04122F.1-1	3841	6.9	18.0	0.258	0.0802	0.0007	0.2084	0.0042	2.304	0.053	0.0589	0.0011	102	1201	16
Data not used (*discordant or >1% common Pb*)[f]															
04122E.1-2	3426	4.2	12.1	0.139	0.0800	0.0005	0.1915	0.0037	2.112	0.045	0.0565	0.0010	94	1197	13
04122D.3-1	2283	7.1	31.0	1.537	0.0785	0.0012	0.2076	0.0045	2.247	0.064	0.0633	0.0011	105	1160	31
04122C.4-1	1716	13.9	80.9	2.032	0.0806	0.0015	0.1979	0.0039	2.199	0.063	0.0604	0.0011	96	1211	36
04122A.1-1	1264	15.3	120.8	2.984	0.0800	0.0018	0.2041	0.0043	2.252	0.074	0.0617	0.0011	100	1198	43
04122B.5-1	1329	9.9	74.9	3.164	0.0739	0.0022	0.2111	0.0045	2.152	0.084	0.0605	0.0011	119	1039	61
04122B.1-1	1587	23.4	147.4	3.411	0.0798	0.0022	0.1993	0.0041	2.192	0.081	0.0557	0.0011	98	1191	54
04122F.1-3	1618	8.7	53.8	3.431	0.0833	0.0032	0.2163	0.0064	2.485	0.128	0.0623	0.0011	99	1276	74
04122E.1-1	648	15.0	231.7	6.660	0.0771	0.0038	0.1763	0.0048	1.873	0.113	0.0562	0.0010	93	1123	98
Sample 9306/011 (Ky-St-Bt-Ms-Qtz schist; assemblage 4)															
Inclusion in biotite porphyroblast															
0557A.1-1	8320	3.6	4.3	0.140	0.0803	0.0003	0.2074	0.0021	2.296	0.023	0.0641	0.0006	101	1204	8
0557A.1-2	4254	2.3	5.5	0.194	0.0803	0.0004	0.2032	0.0020	2.251	0.023	0.0613	0.0006	99	1206	9
In matrix aligned with D4 fabric that wraps the biotite porphyroblast															
0557A.2-1	5555	3.7	6.7	0.110	0.0798	0.0003	0.2039	0.0020	2.242	0.022	0.0624	0.0006	100	1191	8
0557A.2-2	4725	3.5	7.3	0.204	0.0799	0.0005	0.2078	0.0021	2.290	0.023	0.0631	0.0006	102	1195	13
Sample EMB-01 (Ky-Ms-Qtz schist; assemblage 9)															
0557B.1-2	4166	3.9	9.3	0.287	0.0796	0.0004	0.2026	0.0020	2.223	0.022	0.0621	0.0006	100	1187	11
0557C.2-1	7013	4.6	6.6	0.212	0.0792	0.0003	0.2042	0.0020	2.230	0.022	0.0626	0.0006	102	1177	9
0557C.2-2	8640	5.9	6.8	0.148	0.0799	0.0003	0.2034	0.0020	2.240	0.022	0.0624	0.0006	100	1194	8
0557D.1-1	4419	4.0	9.1	0.276	0.0793	0.0004	0.2043	0.0020	2.232	0.022	0.0623	0.0006	102	1179	11
0557D.1-2	5335	4.8	9.0	0.305	0.0794	0.0004	0.2043	0.0020	2.237	0.022	0.0620	0.0006	101	1183	10
Sample 9305/039 (Grt-St-Bt-Ms-Qtz schist; assemblage 2)															
Inclusion in garnet porphyroblast															
0548A.1-1	2112	5.2	24.5	0.447	0.0807	0.0006	0.2075	0.0021	2.308	0.023	0.0645	0.0006	100	1214	14
Distinct cores															
0547A.1-2	2055	4.6	22.6	0.435	0.0807	0.0006	0.2026	0.0020	2.255	0.023	0.0621	0.0006	98	1215	15
0548F.1-1	2373	7.6	31.9	0.502	0.0814	0.0007	0.2095	0.0021	2.351	0.024	0.0669	0.0007	100	1231	16
Outer zones or undefined zoning															
0547A.1-1	2389	6.0	25.2	0.230	0.0790	0.0005	0.1996	0.0020	2.174	0.022	0.0620	0.0006	100	1172	12
0547A.2-2	2250	4.3	19.3	0.241	0.0805	0.0005	0.1985	0.0020	2.203	0.022	0.0616	0.0006	97	1209	13
0547B.1-1	2150	5.4	24.9	0.345	0.0802	0.0005	0.1985	0.0020	2.193	0.022	0.0606	0.0006	97	1201	13
0547B.1-2	3034	1.8	5.8	0.589	0.0798	0.0006	0.1991	0.0020	2.191	0.022	0.0605	0.0006	98	1193	14

(*continued on next page*)

Table 3 (*continued*)

Analysis spot[a]	U (ppm)	Th (%)	Th/U	f206[b] (%)	$^{207}Pb^*/^{206}Pb^*$[c]	±	$^{206}Pb^*/^{238}U$	±	$^{207}Pb^*/^{235}U$	±	$^{208}Pb^*/^{232}Th$	±	Conc.[d] (%)	$^{207}Pb^*/^{206}Pb^*$[e] Age (Ma)	± (Ma)
0547B.2-1	2016	4.3	21.6	0.484	0.0802	0.0006	0.2016	0.0020	2.229	0.022	0.0608	0.0006	99	1201	15
0547B.2-2	1827	4.6	24.9	0.793	0.0811	0.0008	0.2006	0.0020	2.242	0.025	0.0615	0.0006	96	1223	19
0547C.1-1	1252	1.6	12.6	0.450	0.0796	0.0008	0.2018	0.0020	2.216	0.026	0.0608	0.0006	100	1188	20
0547C.2-1	1425	2.5	17.7	0.581	0.0784	0.0008	0.2034	0.0020	2.200	0.025	0.0604	0.0006	103	1158	19
0547C.3-1	1077	1.9	17.9	0.537	0.0813	0.0012	0.2019	0.0020	2.262	0.036	0.0608	0.0006	97	1228	28
0548B.1-1	1253	2.0	16.3	0.280	0.0801	0.0007	0.2144	0.0021	2.367	0.024	0.0653	0.0007	105	1198	17
0548C.1-1	2554	2.7	10.5	0.248	0.0799	0.0005	0.2138	0.0021	2.354	0.024	0.0674	0.0007	105	1194	12
0548E.1-1	1730	1.6	9.2	0.213	0.0809	0.0006	0.2051	0.0021	2.287	0.023	0.0659	0.0007	99	1218	14
0548F.1-2	2371	6.9	29.0	0.693	0.0802	0.0006	0.2141	0.0021	2.369	0.024	0.0642	0.0006	104	1203	16
0548G.1-1	1500	2.8	18.4	0.761	0.0798	0.0008	0.2116	0.0021	2.328	0.028	0.0660	0.0007	104	1191	21
0548H.2-1	2410	8.5	35.3	0.696	0.0805	0.0007	0.2106	0.0021	2.338	0.023	0.0659	0.0007	102	1210	17
0548H.2-2	2252	8.1	36.0	0.574	0.0804	0.0006	0.2121	0.0021	2.351	0.024	0.0659	0.0007	103	1207	16
0548I.1-2	1883	4.9	26.1	0.371	0.0802	0.0006	0.2122	0.0021	2.345	0.023	0.0654	0.0007	103	1201	14
Distinct cores, but >1% common Pb															
0547A.2-1	2165	14.3	66.1	1.092	0.0805	0.0008	0.1986	0.0020	2.204	0.025	0.0624	0.0006	97	1209	21
0548I.1-1	1922	13.6	70.9	1.162	0.0804	0.0008	0.2063	0.0021	2.289	0.027	0.0658	0.0007	100	1208	21
High common Pb															
0548H.1-1	2197	4.4	20.0	20.997	0.0829	0.0041	0.2258	0.0023	2.582	0.131	0.0609	0.0006	104	1268	97
Sample WB-04 (Grt-Bt-Ms-Qtz schist; assemblage 1)															
0549B.1-1	4908	1.4	2.8	0.019	0.0802	0.0003	0.2072	0.0021	2.290	0.023	0.0632	0.0006	101	1201	8
0549B.1-2	3184	2.5	7.7	0.321	0.0801	0.0005	0.2070	0.0021	2.287	0.023	0.0634	0.0006	101	1200	12
0549C.1-1	2965	5.9	20.1	0.046	0.0806	0.0004	0.2049	0.0020	2.277	0.023	0.0630	0.0006	99	1212	9
0549D.1-1	6284	6.3	10.0	0.094	0.0799	0.0003	0.2072	0.0021	2.284	0.023	0.0635	0.0006	102	1195	8
0549F.1-1	4316	5.7	13.2	0.207	0.0796	0.0004	0.2069	0.0021	2.270	0.023	0.0634	0.0006	102	1186	10
0549F.1-2	3409	6.5	19.0	0.146	0.0798	0.0004	0.2063	0.0021	2.271	0.023	0.0645	0.0006	101	1193	10
0549G.1-1	3333	5.7	17.2	0.106	0.0796	0.0004	0.1924	0.0019	2.112	0.021	0.0558	0.0006	96	1187	10
0549G.1-2	7323	5.7	7.9	0.073	0.0797	0.0004	0.1917	0.0019	2.106	0.021	0.0543	0.0005	95	1189	9
0549L.1-1	3293	6.2	19.0	0.158	0.0800	0.0004	0.2055	0.0021	2.267	0.023	0.0637	0.0006	101	1197	10
0549L.1-2	1665	6.3	38.0	0.212	0.0801	0.0005	0.2088	0.0021	2.305	0.023	0.0631	0.0006	102	1199	13

[a] Analysis labels have the form [C]nnnX.p-q, where [C]nnn = UWA mount number, X = disc of thin section in the mount, p = grain in the disc, and q = analysis point in the grain.
[b] 4f206 is the proportion of ^{206}Pb determined to be common Pb, on the basis of measured $^{204}Pb/^{206}Pb$.
[c] All Pb data listed are corrected for common Pb on the basis of measured $^{204}Pb/^{206}Pb$ and a common Pb composition calculated from the Stacey and Kramers (1975) growth curve at the age determined from each analysis.
[d] Conc. is apparent concordance, defined as $100\{t[^{206}Pb/^{238}U]/t[^{207}Pb/^{206}Pb]\}$.
[e] All listed uncertainties are 1σ.
[f] Analyses with >1% common Pb or >5% of apparent discordance were considered unviable for age determinations.

names and mount numbers are listed in Table 3. The monazite was analyzed in situ using a sensitive high-resolution ion microprobe (SHRIMP). Mount 04-122 was analyzed in a 1-day session, and most other mounts (05-47, 05-48, 05-49, 05-57 and 96-35) were analyzed in a single 2-day session. Two analyses of mount 96-35 and four analyses of mount 05-59 were obtained previously in conjunction with other analyses.

The SHRIMP analytical procedures followed established methodologies (Foster et al., 2000; Rasmussen et al., 2001) using ~0.25 nA O_2^- primary ion beams focussed onto ⩽10 μm spots. Monazite standards were set in separate mounts that were gold-coated in conjunction with the sample mounts in each case. The primary Pb/U standard was MAD 1 (Foster et al., 2000; also known in-house as French). Matrix effects on Pb/U data from U and Th were determined using PD-95 (high U; Th generally higher than MAD; provided by J. Aleinikoff) QMa28-1 (U similar to MAD, but with lower Th; provided by F. Henjes-Kunst), and 2908 (moderate U and Th; provided by Richard Stern). For the 2-day analytical session, Pb/U reproducibility for MAD-1 was unusually good, leading to unrealistically low estimates of precision for Pb/U in the unknowns. A "typical best" lower limit of 1% was applied. The $^{207}Pb/^{206}Pb$ data for PD-95 were also used to normalise this ratio for the sample data.

All SHRIMP data are listed in Tables 3 and 4. The precisions shown for $^{207}Pb/^{206}Pb$ include the relatively small uncertainty propagated with the re-normalisation of this ratio. Data without this additional uncertainty were used when calculating $^{207}Pb/^{206}Pb$ averages, and the additional uncertainty applied to the averages determined within each analytical session. The weighted mean dates given in the text have 95% confidence limits. When individual analyses are quoted, the 1σ values from Tables 3 and 4 are used.

Table 4
Summary of SHRIMP U–Pb age data for monazite extracted from mineral separates of sample WBCH1

Analysis Spot	U (ppm)	Th (%)	Th/U	f206 (%)	$^{207}Pb^*/^{206}Pb^*$	±	$^{206}Pb^*/^{238}U$	±	$^{207}Pb^*/^{235}U$	±	$^{208}Pb^*/^{232}Th$	±	Conc. (%)	$^{207}Pb^*/^{206}Pb^*$	
														Age (Ma)	± (Ma)
Mount 96-35 (garnet concentrate; Grt-St-Bt-Ms-Qtz schist?; assemblage 2?)															
9635.10-1	459	3.0	65.8	0.331	0.0705	0.0012	0.1651	0.0049	1.604	0.057	0.0508	0.0010	105	942	36
9635A.1-1	220	1.0	45.7	0.297	0.0693	0.0014	0.1561	0.0021	1.492	0.038	0.0464	0.0005	103	908	42
9635C.1-1	386	2.0	52.9	0.000	0.0701	0.0008	0.1566	0.0016	1.513	0.025	0.0484	0.0005	101	930	24
9635C.1-2	547	3.1	56.9	0.052	0.0716	0.0007	0.1618	0.0016	1.598	0.022	0.0503	0.0005	99	975	20
9635D.1-1	602	2.5	42.2	0.025	0.0727	0.0008	0.1605	0.0021	1.610	0.030	0.0492	0.0005	95	1007	23
9635D.1-2	272	1.3	49.3	0.233	0.0713	0.0012	0.1616	0.0020	1.589	0.034	0.0486	0.0005	100	966	34
9635F.1-1	428	1.0	22.4	0.404	0.0677	0.0013	0.1485	0.0022	1.385	0.034	0.0459	0.0005	104	858	39
Data not used (*discordant*)															
9635.16-1	276	2.0	72.5	0.036	0.0718	0.0008	0.1505	0.0038	1.490	0.043	0.0460	0.0009	92	981	22
9635B.1-1	284	1.7	59.4	0.685	0.0697	0.0018	0.1650	0.0020	1.586	0.046	0.0500	0.0005	107	919	52
9635E.1-1	279	3.4	121.8	0.412	0.0681	0.0013	0.1587	0.0020	1.490	0.036	0.0491	0.0005	109	872	40
Mount 05-59 (staurolite concentrate; Grt-St-Bt-Ms-Qtz schist?; assemblage 2?)															
Monazite inclusion in staurolite															
0559A.1-1	1851	14.5	78	0.000	0.0738	0.0005	0.1720	0.0027	1.750	0.032	0.0567	0.0019	99	1035	15
0559A.1-2	1601	10.8	67	0.000	0.0742	0.0006	0.1706	0.0027	1.746	0.031	0.0543	0.0017	97	1047	16
Monazite inclusion in garnet															
0559B.1-1	1358	3.5	26	0.011	0.0734	0.0006	0.1719	0.0029	1.741	0.034	0.0536	0.0017	100	1026	17
0559B.1-2	2159	6.6	31	0.062	0.0735	0.0006	0.1715	0.0028	1.738	0.033	0.0517	0.0016	99	1027	17

See footnotes for Table 3.

4. Results

4.1. Monazite distribution and textural relationships

Metamorphic monazite is abundant in most samples examined by SEM (Table 1). It is evenly distributed throughout many thin sections of pelitic schists representing a wide range of bulk compositions in AFM space. Monazite crystals are typically idioblastic and range up to 100 μm in length and 30 μm in width. Monazite occurs in the matrix of pelitic schists and as inclusions in porphyroblasts of staurolite, garnet, kyanite, muscovite, biotite and magnetite. In the matrix, elongate monazite crystals are commonly aligned with the main mineral fabric (S_4) (Figs. 5a–d and 6a–d), and less commonly with the earlier S_2 fabric (Fig. 7a, c and e). Monazite also occurs as inclusions within garnet, where it is aligned with quartz and ilmenite that define an earlier S_2 fabric. These observations indicate that monazite growth was synchronous with the development of the two main deformational fabrics. In some samples, coarse biotite porphyroblasts have overprinted monazite aligned in the S_4 fabric (Fig. 5c and d), suggesting that monazite growth occurred before the biotite. However, in other samples, monazite is clearly aligned with, and has grown along, the mineral cleavage of biotite crystals that overprint S_4 (Fig. 6e and f), indicating that some monazite growth was synchronous with, or possibly post-dated the last deformation fabric.

4.2. Chemical zoning in monazite

X-ray element mapping of monazite grains from eight samples shows that most crystals display compositional zonation. The zoning patterns are highly variable within and between samples, and range from concentric to irregular. Compositional zoning is most pronounced in sample WB-01, where monazite crystals typically have a La- and Y-poor and Th-rich core, surrounded by a La- and Y-rich and Th-poor rim (Fig. 8). In some crystals, the core comprises up to three compositionally distinct zones, including an inner zone with intermediate La and Th contents, surrounded by a La-poor, Th-rich middle zone, and a La-rich, Th-poor outer zone. In some places, the growth of the outer rim of the monazite grains has been restricted by adjacent ilmenite crystals, which are aligned with S_4 (Fig. 9), indicating that the final phase of monazite growth probably postdated the development of the S_4 fabric.

4.3. Monazite geochronology

In situ SHRIMP U–Pb analyses were carried out on six samples of pelitic schist and micaceous quartzite from the Mount Barren Group (Tables 2 and 3). Where possible, the analyses were conducted within individual compositional zones to establish whether the compositionally distinct zones identified by WDS element mapping represent different generations of monazite growth. Seventy-one analyses were conducted on samples from the Mount Barren Group, producing $^{207}Pb/^{206}Pb$ dates from 1231 Ma to 1158 Ma (Table 3). A further 14 analyses on sample WBCH1 gave $^{207}Pb/^{206}Pb$ dates between 1047 Ma and 858 Ma (Table 4).

4.3.1. In situ SHRIMP analysis of monazite in metapelitic rocks from the Mount Barren Group

From sample WB-01 (Qtz-Bt-Ms-Ky schist; assemblage 5), 20 analyses of 12 monazite grains yield a unimodal $^{207}Pb/^{206}Pb$ distribution centred at ~1200 Ma, which does not represent a single population (MSWD = 2.3). Many of the monazite grains are aligned with S_4, which is defined by parallel ilmenite, quartz and muscovite crystals. The monazite crystals occur in the quartz-muscovite matrix and as inclusions in coarse biotite and ilmenite crystals that overprint the S_4 fabric (Fig. 5e and f). Element maps show concentric compositional zoning in most monazite grains from this sample (Fig. 8). Division of individual analysis sites into cores (with up to three compositional zones) and rims (single zone) produces weighted mean $^{207}Pb/^{206}Pb$ ages of 1211 ± 13 Ma (MSWD = 1.6; $n = 9$) for the cores, and 1187 ± 10 Ma (MSWD = 0.59; $n = 11$) for the rims (Fig. 10).

Twenty analyses of fifteen monazite crystals from assemblage 2 in sample 9305/039 (Grt-St-Bt-Ms-Qtz), which should have grown monazite at ~1030 Ma according to the hypothesis of Fitzsimons et al. (2005), produced a weighted mean $^{207}Pb/^{206}Pb$ age of 1202 ± 8 Ma (MSWD = 1.3). Most monazite grains occur as inclusions within coarse overprinting biotite, although some are present along grain boundaries, in the matrix (comprising biotite, muscovite and quartz) or as inclusions in garnet. Compositional zoning is present, though less pronounced than in WB-01, and reveals dissolution-type textures in many of the grains. The single inclusion in garnet and two cores that can be unambiguously differentiated give a weighted mean $^{207}Pb/^{206}Pb$ age of 1219 ± 15 Ma, whereas grains and zones that cannot be differentiated give an age of 1198 ± 9 Ma (MSWD = 1.2).

Four analyses of two monazite crystals in sample 9306/011 (Ky-St-Bt-Ms-Qtz; assemblage 4) give ages ~1200 Ma, consistent with results from other samples. One of the crystals is aligned with an earlier fabric (S_2?) that is preserved within a biotite porphyroblast that is wrapped by the main S_4 fabric. The second grain occurs in the matrix and is aligned with the S_4 fabric. The individual analyses of the texturally earlier monazite gives ages of 1206 ± 9 Ma and 1204 ± 8 Ma, whereas the matrix monazite gives ages of 1195 ± 13 Ma and 1191 ± 8 Ma (all dates 1σ).

Ten analyses of six monazite crystals in sample WB-04 (Grt-Bt-Ms-Qtz; assemblage 1) yield a weighted mean $^{207}Pb/^{206}Pb$ age of 1196 ± 10 Ma (MSWD = 1.1). The monazite in this sample is idioblastic, and is typically aligned with a strong S_4 cleavage defined by muscovite, quartz and ilmenite. The monazite crystals are typically <20 μm, and display concentric compositional zoning. Be-

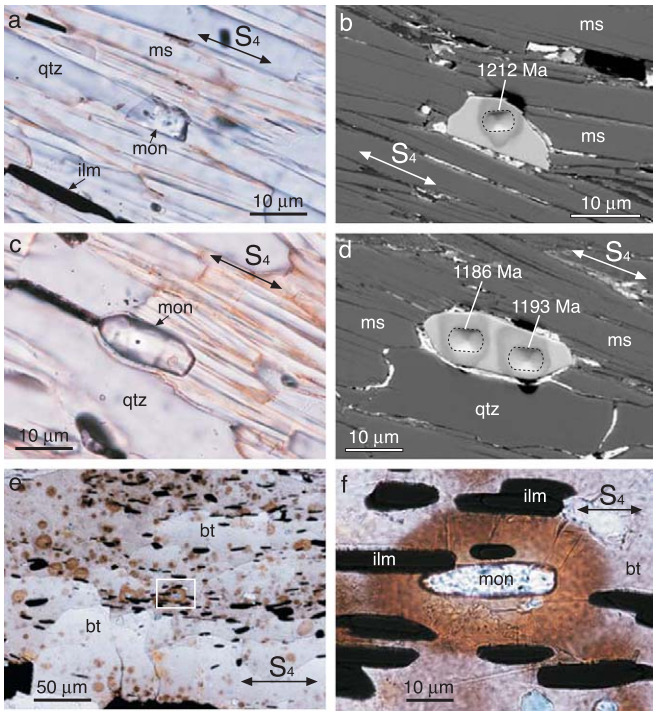

Fig. 5. (a) Optical photomicrograph of monazite (mon) crystal parallel with the dominant S_4 fabric defined by aligned quartz (qtz), muscovite (ms) and ilmenite (ilm); (b) back-scattered electron (BSE) image of idioblastic monazite aligned with the S_4 fabric marked by near-parallel muscovite (ms) crystals. Single SHRIMP pit corresponds with analysis spot 0549C.1-1 in Table 3; (c) elongate monazite (mon) in matrix aligned with S_4 fabric; (d) BSE image of idioblastic monazite parallel to muscovite and quartz aligned with S_4. Two SHRIMP pits correspond with analysis spots 0549F.1-1 and 0549F.1-2 in Table 3; (e) coarse biotite crystal that overprints the S_4 fabric defined by inclusions of ilmenite (opaque) and radioactive mineral inclusions (with pleochroic haloes); (f) closeup of inset in previous photograph showing an elongate monazite crystal aligned in the S_4 fabric and parallel with ilmenite inclusions. Note the well-developed pleochroic halo, which is typical of monazite in biotite. (a–d) From sample WB-04; (e) and (f) are from sample WB-01.

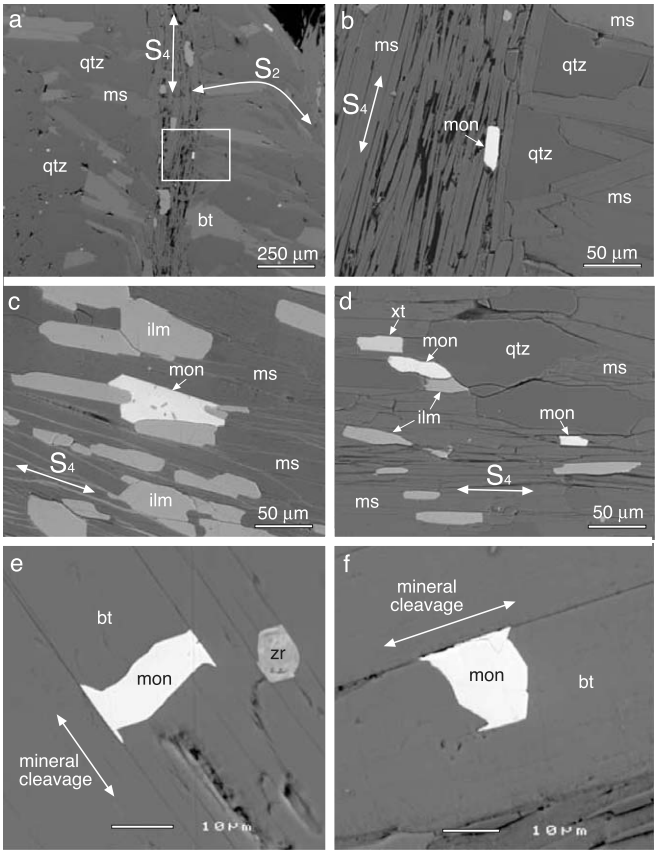

Fig. 6. BSE images showing (a) crenulation cleavage in pelitic schist with the S_4 foliation defined by cleavage domains (defined mainly by muscovite) and microlithons preserving the S_2 fabric defined by muscovite, quartz and biotite; (b) closeup of (a) showing an idioblastic monazite grain parallel to S_4 defined by muscovite; (c) monazite grain containing small randomly oriented ilmenite (ilm) inclusions that is parallel to S_4 defined by parallel coarse ilmenite, muscovite (ms) and quartz (qtz); (d) elongate monazite (mon) and xenotime (xt) parallel to S_4 fabric defined by muscovite, ilmenite and quartz; (e) and (f) monazite (mon) inclusion within a coarse biotite crystal that overprints the S_4 fabric. Note the growth of monazite parallel to mineral cleavage. (a, b, e and f) From sample BB-03; (c) is from sample WB-01; (d) is from sample 9306/018.

cause of the fine scale of the zoning it was not possible to analyze individual zones, and consequently, the date is possibly a mixture between ~1210 Ma and ~1185 Ma populations.

Five analyses of three monazite crystals in sample EMB-01 (Ky-Ms-Qtz; assemblage 9) conform to a single population, with a mean $^{207}Pb/^{206}Pb$ age of 1185 ± 8 Ma (MSWD = 1.1). All three crystals occur in the quartz-muscovite matrix.

4.3.2. SHRIMP analysis of monazite from mineral separates (WBCH1)

Ten analyses of eight monazite crystals separated from sample WBCH1 (Grt-St-Bt-Ms-Qtz; assemblage 2) yield dates that are scattered, and consistent with earlier analyses by Wetherley (1998). Eight of these analyses are of previously undated monazite, some of which is intergrown with allanite. These produced a wide scatter, from 858 ± 38 Ma to 1007 ± 22 Ma (1σ) (Table 4). Monazite analyses from this mount have given dates spanning ~200 m.y. (from ~1050 Ma to ~850 Ma), with no clearly defined age populations and a strong relationship between Th content (at <5 wt% Th) and apparent age (Fig. 11).

Two new SHRIMP mounts were made of garnet (05-58) and staurolite (05-59) concentrates from sample WBCH1. The garnet mount contained over 400 fragments whereas the staurolite mount contained ~700 fragments. The garnet and staurolite fragments contain abundant inclusions of ilmenite, zircon, quartz and apatite, with minor tourmaline and muscovite. The garnet mount also contained very rare allanite and thorite, whereas a staurolite fragment contained a single monazite inclusion. The staurolite mount also contained about 10 garnet fragments, two of which contained monazite inclusions. In situ analysis of the largest monazite inclusion in garnet yielded dates of 1026 ± 17 Ma and 1027 ± 17 Ma, whereas the monazite inclusion in staurolite gave dates of 1047 ± 16 Ma and

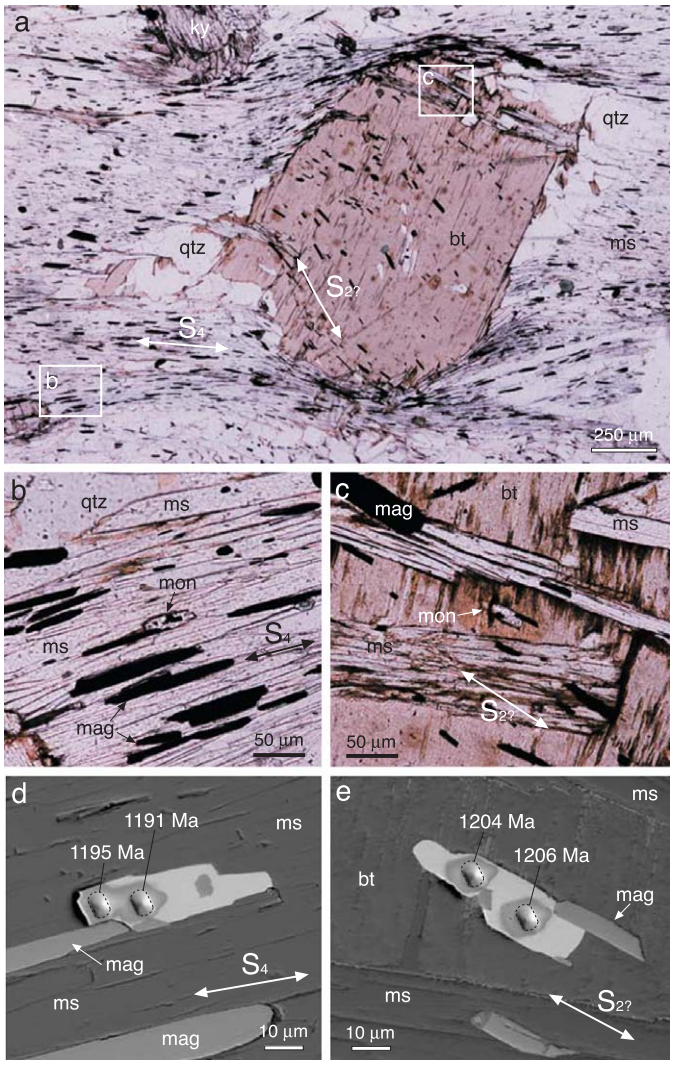

Fig. 7. (a) Optical photomicrograph of a coarse biotite crystal in a pelitic schist wrapped by S_4 foliation and with asymmetric strain shadows (marked by quartz); (b) optical photomicrograph of monazite (mon) aligned with S_4 fabric defined by Ti-magnetite (mag), muscovite (ms) and quartz (qtz) crystals; (c) optical photomicrograph of monazite (mon) surrounded by a pleochroic halo aligned with an early S_2? fabric defined by Ti-magnetite (mag) inclusions; (d) BSE image of the elongate monazite (mon) crystal shown in (b) with two SHRIMP pits corresponding with analysis spots 0557A.2-1 and 0557A.2-2 in Table 3; (e) BSE image of the elongate monazite (mon) crystal shown in (c) with two SHRIMP pits corresponding with analysis spots 0557A.1-1 and 0557A.1-2 in Table 3. Sample 9306/011. The SHRIMP ages are consistent with the relative ages of S_2 and S_4 determined from textural relationships.

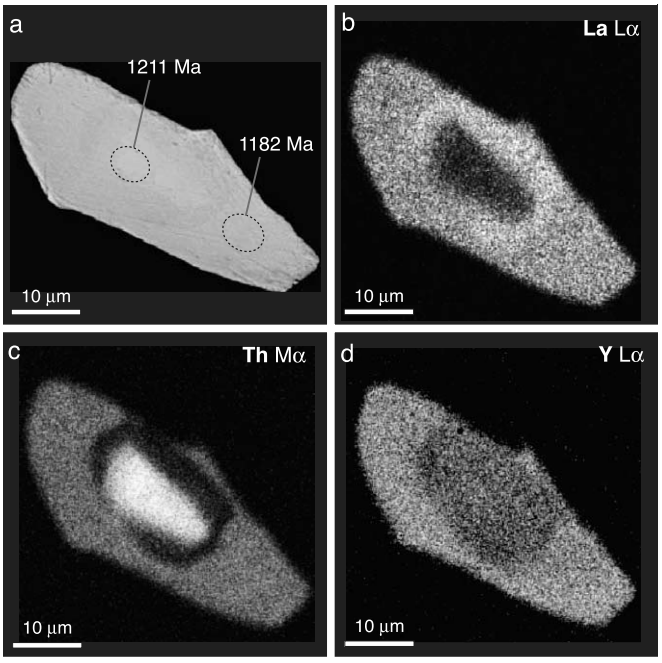

Fig. 8. (a) BSE image of a monazite showing location of two SHRIMP analytical pits (analysis spots 04122C.4-1 and 04122C.4-2; Table 3) and their corresponding $^{207}Pb/^{206}Pb$ ages; (b–d) corresponding wavelength dispersive X-ray maps for (b) La, (c) Th and (d) Y. The element maps define a La-poor, Th-rich core, enclosed by a thin zone of La-rich and Th-poor monazite, surrounded by a relatively thick La-rich, Th-poor rim. The outer rim corresponds with a slight enrichment of yttrium. Sample WB-01.

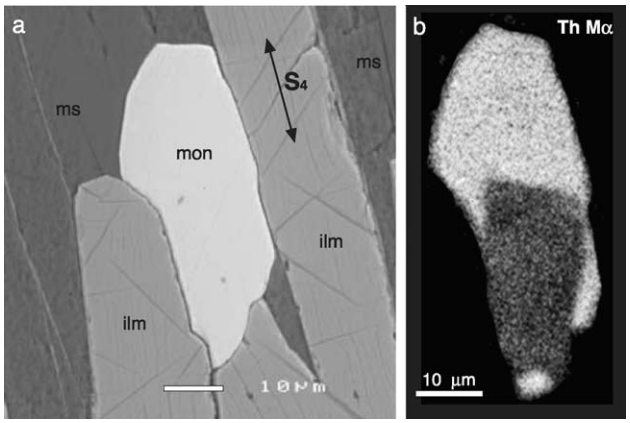

Fig. 9. (a) BSE image of monazite (mon) wedged between ilmenite crystals parallel with the S_4 foliation; (b) Wavelength dispersive X-ray map for Th showing a Th-poor core surrounded by a Th-rich rim. Note the asymmetric growth of the Th-rich monazite rim, suggesting growth after formation of the S_4-aligned ilmenite. Sample WB-01.

1035 ± 15 Ma (Table 4). Together these analyses give a weighted mean $^{207}Pb/^{206}Pb$ date of 1035 ± 15 Ma (MSWD = 0.45).

5. Discussion

5.1. In situ U–Pb age constraints on the timing of peak metamorphism

Monazite from the Mount Barren Group occurs in the matrix and as inclusions within porphyroblasts of garnet, staurolite, kyanite, biotite, muscovite and magnetite in *a wide range of bulk compositions in AFM space*. In situ SHRIMP U-Pb dating of monazite in five samples of pelitic schist and micaceous quartzite (Table 3) produced dates with a mean $^{207}Pb/^{206}Pb$ age of ~1200 Ma, confirming the findings of Dawson (2000) and Dawson et al. (2003). There is significant scatter in the monazite age data (MSWD = 1.8), which suggests that there may be more

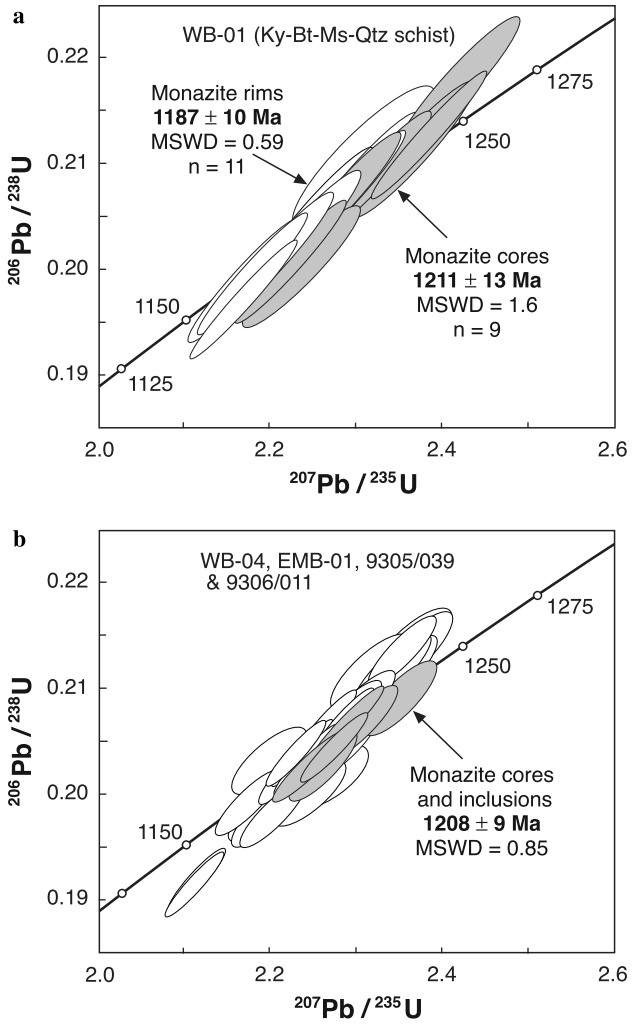

Fig. 10. Concordia plots showing SHRIMP U–Pb data for metamorphic monazite from (a) sample WB-01, which contains compositionally distinct cores (light grey) and rims (white), and (b) samples WB-04, EMB01, 9305/039 and 9306/011. In (b), monazite cores and inclusions within garnet are plotted as shaded ellipses. Some data fall outside the plotted fields (see Table 3). MSWD denotes mean squares of weighted deviates. Age uncertainties are 95% confidence limits and individual precision ellipses are 1σ.

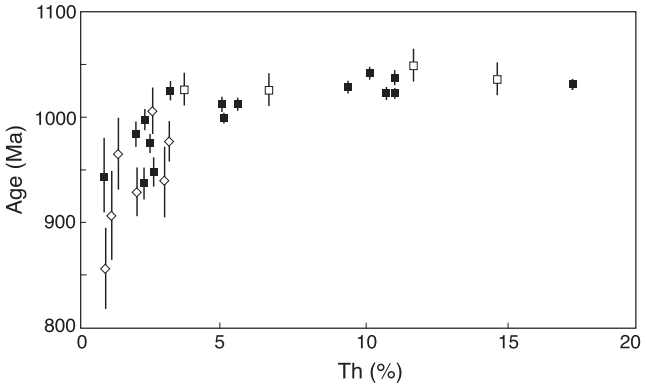

Fig. 11. Plot showing correlation between $^{207}Pb/^{206}Pb$ dates and Th content for monazite from sample WBCH1. Data are from Wetherley (1998) (mount 96-35; black squares) and this study (mount 96-35—white diamonds; mount 05-59—white squares). Age uncertainties are 1σ.

than one age population. In sample WB-01, compositionally distinct rims yield a discrete population of 1187 ± 10 Ma. Combining this with 1185 ± 8 Ma for the single-aged, texturally "late" monazite (sample EMB-01) gives a date of 1186 ± 6 Ma (MSWD = 0.8) for the youngest discrete monazite growth event. In sample WB-01, the growth of rims has been affected by adjacent ilmenite aligned with S_4, suggesting that the ~1185 Ma monazite rim formed syn- to post-S_4. Thus, we consider 1186 ± 6 Ma as the likely timing of peak thermal metamorphism in the Mount Barren Group. In contrast, combining all data for the monazite cores and the inclusions in porphyroblasts preserving a pre-S_4 foliation (from sample WB-01, 9305/039 and 9306/011) yields a less well defined age of 1209 ± 10 Ma (MSWD = 1.2), which we interpret as the age of pre-S_4 prograde metamorphism. Other data average ~1195 Ma, but it is unclear whether these data are age mixtures or whether they represent an additional discrete stage of monazite growth. The separation of the age data into two populations (~1210 Ma and ~1185 Ma) is supported by unmixing models (Sambridge and Compston, 1994), which yield peaks at ~1207 Ma and ~1190 Ma. This suggests that prograde metamorphism spanned at least 25 million years.

5.2. Implications for previous work

Fitzsimons et al. (2005) argued that the ~1200 Ma monazite and xenotime crystals dated by Dawson et al. (2003) are inclusions within biotite (aligned with S_4), and therefore must be older than the enclosing mica and the F_4 folding event. However, we have shown that monazite is aligned with S_4, suggesting that ~1200 Ma growth was coincident with the last major deformational event. Furthermore, monazite also grew along the cleavage planes of coarse biotite crystals (Fig. 6e and f) that overprint S_4, indicating that some monazite growth continued during and after the development of the S_4 fabric. Thus, our results show that ~1200 Ma monazite growth can be linked to peak deformation (D_4) and peak metamorphism, and is not related to an earlier greenschist facies event as concluded by Fitzsimons et al. (2005).

Our results provide no evidence for the growth of monazite in the Mount Barren Group at ~1030 Ma. Instead, about seventy in situ U–Pb analyses of monazite from six samples, including a sample with assemblage 2 that should contain ~1030 Ma monazite according to the reasoning of Fitzsimons et al. (2005), all give dates between ~1230 Ma and ~1160 Ma. All the younger dates recorded (~1050–850 Ma) are from monazites in mineral separates from a single sample (WBCH1). We have endeavored to locate this sample in order to verify the presence of ~1030 Ma monazite and ascertain its textural relationships. Unfortunately, there is no hand specimen or thin section available from this sample—all that remains is a SHRIMP mount

(96-35) and several vials containing heavy mineral concentrates. The field locality of the sample has not been recorded although it is thought to have come from West Beach (S. Wetherley, pers comm., 2005).

Examination of the SHRIMP mount (96-35), as well as mounts 05-58 (garnet separates) and 05-59 (staurolite separates) from WBCH1, shows that monazite occurs as: (i) isolated grains amongst fragments of allanite, staurolite, quartz and garnet (Fig. 12a and b), (ii) irregular grains sharing crystal boundaries with allanite, chlorite, ilmenite and/or plagioclase (Fig. 12c–e), and (iii) inclusions in unaltered garnet and staurolite fragments (Fig. 12f and g). The intimate association of monazite with allanite in mount 96-35 has not been described previously in schists from the Mount Barren Group (Hollingsworth, 1996; Stephens, 1996; Wetherley, 1998; Dawson et al., 2003; Fitzsimons et al., 2005) nor observed in this study, and may point to a retrograde origin for the younger monazite (~950–850 Ma).

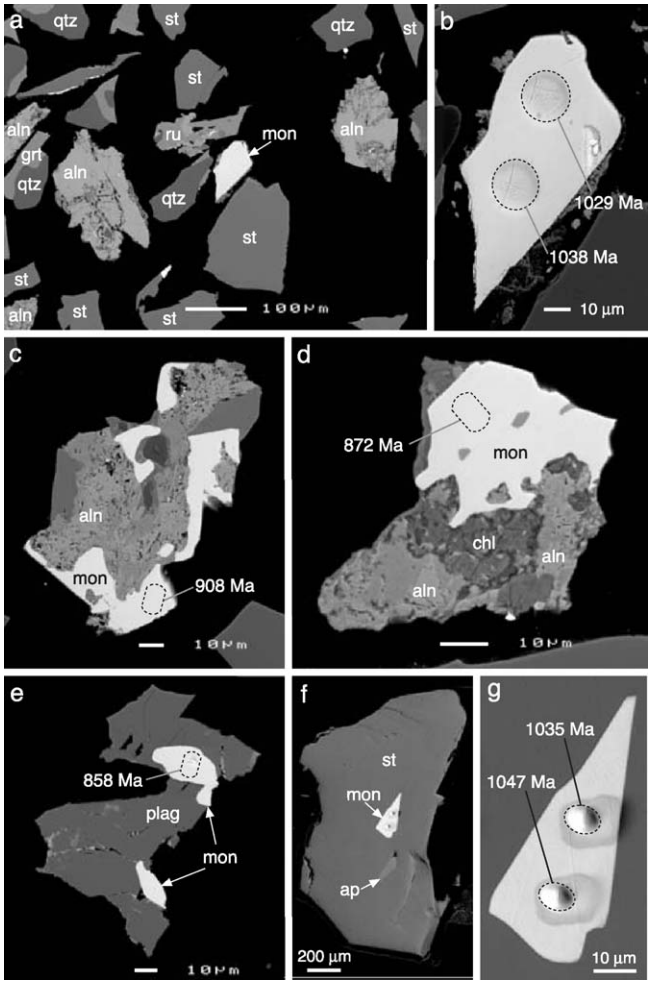

Fig. 12. BSE images of monazite separated from garnet concentrates (SHRIMP mount 96-35; a–e) and staurolite concentrates (SHRIMP mount 05-59; f and g) from sample WBCH1; (a) isolated monazite crystal (white) dated by Wetherley (1998) amongst mainly staurolite (st) and allanite (aln) grains; (b) closeup of monazite in (a), showing two circular SHRIMP analytical pits and related $^{207}Pb/^{206}Pb$ dates. The dates correspond with analyses (a) and (b) in Table 3 of Fitzsimons et al. (2005); (c and d) Irregular monazite (mon) intergrown with allanite and chlorite (chl). (c) and (d) correspond with SHRIMP analyses 9635A.1-1 and 9635E.1-1 (Table 4), respectively; (e) Monazite (mon) crystals within plagioclase (plag). Note that plagioclase has not been reported in samples from this locality. Date corresponds with SHRIMP analysis 9635F.1-1 (Table 4); (f) Monazite (mon) and apatite (ap) inclusions enclosed within a fragment of staurolite (st). (g) Closeup of monazite in (f), showing two oval SHRIMP analytical pits and related $^{207}Pb/^{206}Pb$ dates. Dates correspond with SHRIMP analysis 0559A.1-1 and 0559A.1-2 (Table 4).

The presence of unaltered ~1030 Ma monazite inclusions enclosed within garnet and staurolite fragments from WBCH1 indicates that this generation of monazite must have grown prior to or during amphibolite facies metamorphism. However, we have shown that peak metamorphism occurred at ~1200 Ma. There is no structural or metamorphic record of an amphibolite facies event in pelitic schists from the Mount Barren Group postdating D_4 (Thom, 1977; Hollingsworth, 1996; Stephens, 1996; Witt, 1997, 1998; Wetherley, 1998; Dawson, 2000; Dawson et al., 2003; Fitzsimons et al., 2005). The absence of 1200 Ma monazite in WBCH1, and the absence of 1030–950 Ma monazite in the samples dated by in situ geochronology is difficult to reconcile, and suggests that the younger (1030–950 Ma) monazite grains dated by Fitzsimons et al. (2005) were not derived from West Beach.

5.3. Palaeomagnetic constraints on the timing of peak metamorphism

Palaeomagnetic evidence also argues strongly for a thermal metamorphic peak around 1200 Ma. A dyke of the Fraser swarm (Fig. 1, inset) was dated by Wingate et al. (2000) at 1212 ± 10 Ma. This exposure also yielded a palaeomagnetic baked-contact test, which demonstrates that the dyke carries a primary thermal remanent magnetization (TRM) (Pisarevsky et al., 2003). Metasedimentary rocks of the Mount Barren Group and adjacent granulites of the Biranup Complex yielded two palaeopoles, named MBG and BB1, respectively (Pisarevsky and Harris, 2001; Pisarevsky et al., 2003). These poles fall close to the pole, FDS, for the Fraser dyke (Fig. 13), indicating that all three poles have an age of ~1200 Ma. Four ENE-trending dykes of the ~1215 Ma Gnowangerup swarm (Evans, 1999; Rasmussen and Fletcher, 2004), sampled about 25 km north of the Mount Barren Group exposures, yielded similar palaeomagnetic results (Giddings, 1976). Collectively, these data reliably indicate the position of the pole relative to Australia at about 1210 Ma.

Palaeopoles are also well established for Australia at 1070 Ma and 755 Ma (Wingate and Giddings, 2000; Wingate et al., 2002). These younger poles, however, are located more than 90° from those for 1210 Ma (Fig. 13). The MBG and BB1 poles represent magnetizations acquired during cooling following the thermal peak of metamorphism. The consistency of palaeomagnetic directions determined in samples from different sites in the Mount Barren Group also indicates that their magnetization postdates

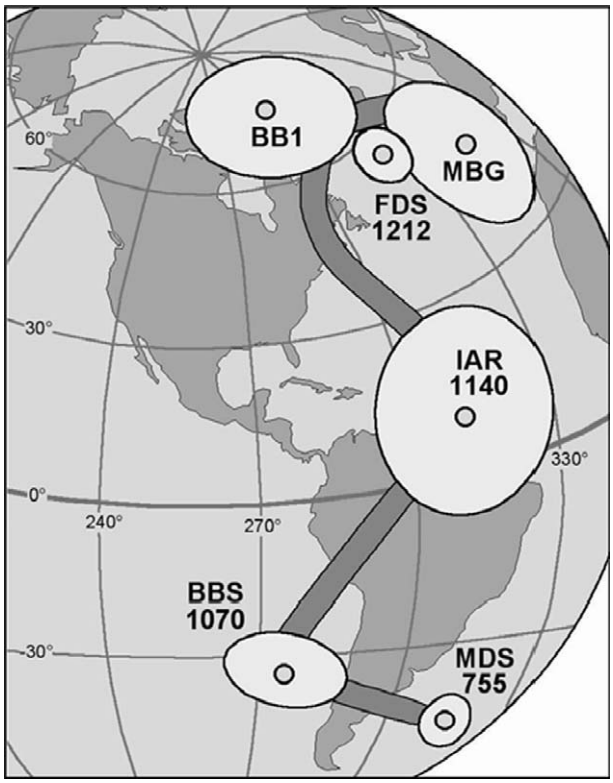

Fig. 13. Late Mesoproterozoic to Neoproterozoic apparent polar wander (APW) path for Australia, in present coordinates. Poles (with A_{95} confidence ovals): FDS, Fraser dyke suite; MBG, Mount Barren Group; BB1, Bremer Bay metamorphic rocks; IAR, Lakeview Dolerite; BBS, Bangemall Superbasin sills; MDS, Mundine Well dykes (Tanaka and Idnurm, 1994; Wingate and Giddings, 2000; Wingate et al., 2002; Pisarevsky et al., 2003). Ages are in Ma.

regional NW-verging thrusting and folding. If the metamorphic thermal peak occurred at 1030 Ma, as suggested by Fitzsimons et al. (2005), then palaeopoles (MBG, BB1) for the metamorphic rocks would be expected to plot close to the 1070 Ma BBS pole, rather than near the 1212 Ma FDS pole. Magnetizations in metamorphic rocks in the Mount Barren Group and adjacent granulites were most likely acquired at ~1200 Ma, and are not consistent with a 1030 Ma thermal peak in the Albany–Fraser orogen.

5.4. Implications for monazite geochronology

Monazite is isotopically robust (Cherniak et al., 2004) and can retain its age information through several episodes of metamorphism, commonly preserving multiple ages within a single grain (DeWolf et al., 1993; Cocherie et al., 1998; Williams et al., 1999; Gibson et al., 2004; Kohn et al., 2005). There is growing recognition of the likely complexity of monazite ages in metamorphic rocks (Lanzirotti and Hanson, 1996; Catlos et al., 2002), and that individual dates may reflect the age of the protolith or provenance, earlier metamorphic events, the timing of prograde, peak and/or retrograde metamorphism, or a later thermal overprint (Lanzirotti and Hanson, 1996; Crowley and Ghent, 1999; Catlos et al., 2001; Foster et al., 2002; Wing et al., 2003). Because of these potential problems, it is crucial to obtain textural evidence linking the timing of monazite growth to deformation and/or metamorphism (Williams and Jercinovic, 2002). Studies that rely on heavy mineral separation techniques lose vital textural information between monazite and the host-rock and can introduce contaminants, making the interpretation of monazite ages exceedingly difficult. This study reinforces the importance of documenting the textural relationship between accessory phases and deformational fabrics and metamorphic minerals, as well as chemical characterization, to identify internal zonation prior to in situ geochronology. Without such an approach, our ability to interpret monazite dates can be seriously flawed.

The growth of monazite during prograde amphibolite facies metamorphism is commonly linked to the breakdown of other accessory phases, particularly allanite (Overstreet, 1967; Smith and Barreiro, 1990; Ferry, 2000; Wing et al., 2003), though reactions amongst common metamorphic silicate minerals, for example the breakdown of garnet to form staurolite, have also been proposed (Kohn and Malloy, 2004). This idea has been extended to argue that bulk composition controls the growth of amphibolite facies monazite, specifically, that monazite only forms in schists that have undergone prograde garnet destruction and staurolite formation (Fitzsimons et al., 2005). The majority of samples do not have the appropriate composition for this reaction to occur, and so do not grow new monazite during peak metamorphism, but rather preserve relicts of an earlier greenschist facies event (~1200 Ma) (Fitzsimons et al., 2005). Our results demonstrate the widespread distribution of peak metamorphic monazite in micaceous quartzite and low-Ca pelitic schists with a wide range of bulk compositions in AFM space. The presence of peak metamorphic monazite in schists that had bulk compositions too Fe-rich (assemblage 1) and too Mg- and/or Al-rich (assemblages 3–6, 9) to undergo garnet breakdown and staurolite formation, demonstrates that variations in bulk composition did not control monazite growth in the samples studied here.

Clearly, the destruction of garnet, muscovite and chlorite was not the source of REE and P for monazite growth in most pelitic schists. The breakdown of accessory minerals such as allanite during prograde metamorphism is also unlikely, because the low-Ca content of the schists does not favour its growth. An alternative source of REE and P in the Mount Barren Group is detrital monazite and xenotime. Greenschist facies metapelites elsewhere in the Mount Barren Group contain detrital monazite and xenotime in heavy mineral bands with zircon and tourmaline. Their absence in amphibolite facies schists, that contain abundant detrital zircon and tourmaline with metamorphic overgrowths, suggests that both REE-phosphates were dissolved during prograde metamorphism. Similarly, diagenetic and low-grade metamorphic xenotime and low-grade metamorphic monazite, which are relatively common in greenschist facies metapelitic rocks from else-

where in the Mount Barren Group (Vallini et al., 2002, 2005; unpub. data), did not survive prograde amphibolite facies metamorphism. Their absence suggests that diagenetic and low-grade metamorphic phosphates were probably also destroyed during prograde metamorphism and acted as potential sources of P and REE for intermediate phases or amphibolite facies monazite and xenotime. Whatever the sources of REE and P for monazite and xenotime, it is clear that no single reaction amongst major silicate phases controlled phosphate growth and that the mechanisms are more varied and complex than often envisaged.

6. Conclusions

The interpretation of monazite ages in metamorphic belts requires careful documentation of textural information and chemical and isotopic zonation. In the Mount Barren Group, the growth of monazite crystals parallel to deformational fabrics and mineral cleavages of post-tectonic mica indicates that monazite growth probably spanned peak deformation and peak metamorphism. In situ U–Pb geochronology of monazite yields ages close to 1200 Ma, consistent with the results of Dawson et al. (2003) and with the known geological history in the Albany–Fraser Orogen and the corresponding Wilkes Province in Antarctica (Fitzsimons, 2003). This age for peak metamorphism is also supported by palaeomagnetic results for the Mount Barren Group, nearby granulite-facies rocks of the Albany–Fraser Orogen, and ~1210 Ma mafic dykes in the bordering craton. Our findings also suggest that there is no foundation for a Stage III tectonic cycle at ~1030 Ma in the Albany–Fraser Orogen.

The ~1200 Ma monazite date displays excess scatter (MSWD = 1.8) and probably does not coincide with a specific metamorphic event, but rather, reflects the average of two or more discrete populations. Element mapping of monazite reveals the presence of distinct cores and rims, which yield two ages: cores give an age of ~1210 Ma, whereas the rims give an age of ~1185 Ma. Textural evidence suggests that ~1210 Ma coincides with prograde metamorphism and deformation, whereas ~1185 Ma corresponds with the thermal peak, which post-dated deformation.

Low-Ca pelitic schists representing a broad range of bulk compositions in AFM space all contain near-peak metamorphic (~1200 Ma) monazite. These results indicate that slight differences in whole-rock composition do not control whether monazite forms in such rocks during amphibolite facies metamorphism as proposed by Fitzsimons et al. (2005). In addition, the reaction involving garnet destruction and staurolite formation, which was considered to be solely responsible for peak metamorphic monazite growth, cannot explain the distribution of monazite in the Mount Barren Group. Clearly, other metamorphic reactions are responsible for monazite growth.

In situ analysis of more than one hundred metamorphic monazite and xenotime grains (Dawson et al., 2003; this study) has provided no evidence for younger generations of monazite in any of the rocks from the Mount Barren Group. The absence of 1030–950 Ma-monazite in this study, and the lack of any textural information or documented sample location for the 1030–950 Ma monazite, makes it difficult to evaluate the significance of these younger dates. Irrespective of the origin of the monazite grains dated by Fitzsimons et al. (2005), they clearly do not record amphibolite facies metamorphism in the Mount Barren Group, which occurred between ~1210 Ma and ~1185 Ma.

Acknowledgments

We thank Galvin Dawson, Neal McNaughton, Steve Sheppard and Simon Wetherley for comments and discussion, and the staff of the University of Western Australia's Centre for Microscopy and Microanalysis for their assistance. We thank CALM for permission to collect samples within the Fitzgerald River National Park. The paper was improved by comments from John Ferry, Simon Harley and an anonymous reviewer. Monazite analyses were performed on the Western Australian SHRIMP II, operated by a WA university-government consortium with ARC support.

Associate editor: T. Mark Harrison

References

Bea, F., Montero, P., 1999. Behavior of accessory phases and redistribution of Zr, REE, Y, Th, and U during metamorphism and partial melting of metapelites in the lower crust: an example from the Kinzigite Formation of Ivrea–Verbano, NW Italy. *Geochim. Cosmochim. Acta* **63**, 1133–1153.

Beeson, J., Delor, C.P., Harris, L.B., 1988. A structural and metamorphic traverse across the Albany Mobile Belt, Western Australia. *Precambrian Res.* **40/41**, 117–136.

Bingen, B., van Breemen, O., 1998. U-Pb monazite ages in amphibolite- to granulite-facies orthogneiss reflect hydrous mineral breakdown reactions: Sveconorwegian Province of SW Norway. *Contrib. Mineral. Petrol.* **132**, 336–353.

Black, L.P., Harris, L.B., Delor, C.P., 1992. Reworking of Archaean and Early Proterozoic components during a progressive, Middle Proterozoic tectonothermal event in the Albany Mobile Belt, Western Australia. *Precambrian Res.* **59**, 95–123.

Bodorkos, S., Clark, D.J., 2004. Evolution of a crustal-scale transpressive shear zone in the Albany–Fraser Orogen, SW Australia: 2. Tectonic history of the Coramup Gneiss and a kinematic framework for Mesoproterozoic collision of the West Australian and Mawson cratons. *J. Metamorphic Geol.* **22**, 713–731.

Catlos, E.J., Gilley, L.D., Harrison, T.M., 2002. Interpretation of monazite ages obtained via in situ analysis. *Chem. Geol.* **188**, 193–215.

Catlos, E.J., Harrison, T.M., Kohn, M.J., Grove, M., Ryerson, F.J., Manning, C.E., Upreti, B.N., 2001. Geochronologic and thermobarometric constraints on the evolution of the Main Central Thrust, central Nepal Himalaya. *J. Geophys. Res.* **106**, 16177–16204.

Chang, L.L.Y., Howie, R.A., Zussman J., 1998. *Rock-Forming Minerals. Volume 5B: Non-Silicates: Sulphates, Carbonates, Phosphates and Halides*. Longman Group, Harlow, UK.

Cherniak, D.J., Watson, E.B., Grove, M., Harrison, T.M., 2004. Pb diffusion in monazite: a combined RBS/SIMS study. *Geochim. Cosmochim. Acta* **68**, 829–840.

Clark, D.J., Kinny, P.D., Post, N.J., Hensen, B.J., 1999. Relationships between magmatism, metamorphism and deformation in the Fraser Complex, Western Australia: constraints from new SHRIMP U–Pb zircon geochronology. *Aust. J. Earth Sci.* **46**, 923–932.

Clark, D.J., Hensen, B.J., Kinny, P.D., 2000. Geochronological constraints for a two-stage history of the Albany–Fraser Orogen, Western Australia. *Precambrian Res.* **102**, 155–183.

Cocherie, A., Legendre, O., Peucat, J.-J., Kouamelan, A.N., 1998. Geochronology of polygenetic monazites constrained by in situ electron microprobe Th-U-total Pb determination: implications for lead behaviour in monazite. *Geochim. Cosmochim. Acta* **62**, 2475–2497.

Condie, K.C., Myers, J.S., 1999. Mesoproterozoic Fraser Complex: geochemical evidence for multiple subduction related sources of lower crustal rocks in the Albany–Fraser Orogen, Western Australia. *Aust. J. Earth Sci.* **46**, 875–882.

Crowley, J.L., Ghent, E.D., 1999. An electron microprobe study of the U–Th–Pb systematics of metamorphosed monazite: the role of Pb diffusion versus overgrowth and recrystallization. *Chem. Geol.* **157**, 285–302.

Dawson, G.C., 2000. The nature and origin of trace phosphates and provenance studies of metasedimentary rocks of the Mount Barren Group, Albany–Fraser Province, Western Australia. BSc (Hons) thesis, Univ. Western Australia.

Dawson, G.C., Krapez, B., Fletcher, I.R., McNaughton, N.J., Rasmussen, B., 2002. Did late Palaeoproterozoic assembly of proto-Australia involve collision between the Pilbara, Yilgarn and Gawler Cratons? Geochronological evidence from the Mount Barren Group in the Albany–Fraser Orogen. *Precambrian Res.* **118**, 195–220.

Dawson, G.C., Krapez, B., Fletcher, I.R., McNaughton, N.J., Rasmussen, B., 2003. 1.2 Ga thermal metamorphism in the Albany–Fraser Orogen of Western Australia: consequence of collision or regional heating by dyke swarms? *J. Geol. Soc. Lond.* **160**, 29–37.

DeWolf, C.P., Belshaw, N., O'Nions, R.K., 1993. A metamorphic history from micron-scale $^{207}Pb/^{206}Pb$ chronometry of Archean monazite. *Earth Planet. Sci. Lett.* **120**, 207–220.

Evans, T., 1999. Extent and nature of the 1200 Ma Wheatbelt dyke swarm, southwestern Australia. BSc (Hons) thesis, Univ. Western Australia.

Ferry, J.M., 2000. Patterns of mineral occurrence in metamorphic rocks. *Am. Mineral.* **85**, 1573–1588.

Fitzsimons, I.C.W., 2003. Proterozoic basement provinces of southern and southwestern Australia and their correlation with Antarctica. In: Yoshida, M., Windley, B.F., Dasgupta, S. (Eds.). *Proterozoic East Gondwana: Supercontinent Assembly and Breakup*. Geological Society, London, Special Publications 206, pp. 93–129.

Fitzsimons, I.C.W., Buchan, C., 2005. Geology of the western Albany-Fraser Orogen, Western Australia—a field guide. Western Australia Geological Survey, Record 2005/11, Perth.

Fitzsimons, I.C.W., Kinny, P.D., 2005. Three stages of Mesoproterozoic metamorphism during crustal shortening in the Albany-Fraser Orogen of SW Australia. In: Wingate, M.T.D., Pisarevsky, S.A. (Eds.). *Supercontinents and Earth Evolution Symposium*. Geol. Soc. Aust. Inc. Abstr. 81, p. 129.

Fitzsimons, I.C.W., Hollingsworth, D.A., Kinny, P.D., Wetherley, S., 2004. Bulk chemical control on metamorphic phosphate growth in pelitic schist of the Mount Barren Group, Western Australia. In: 2004 Joint Asia Oceania Geosci. Soc. 1st Ann. Meeting and 2nd Asia Pacific Assoc. of Hydrology Water Resources Conf., 57-OSE-A1101.

Fitzsimons, I.C.W., Kinny, P.D., Wetherley, S., Hollingsworth, A., 2005. Bulk chemical control on metamorphic monazite growth in pelitic schists and implications for U–Pb age data. *J. Metamorphic Geol.* **23**, 261–277.

Fletcher, I.R., Myers, J.S., Ahmat, A.L., 1991. Isotopic evidence on the age and origin of the Fraser Complex, Western Australia: a sample of Mid-Proterozoic lower crust. *Chem. Geol.* **87**, 197–216.

Fletcher, I.R., Wilde, S.A., Libby, W.G., Rosman, K.J.R., 1983. Sm–Nd model ages from across the margins of the Archaean Yilgarn Block, Western Australia, II: southwest transect into the Proterozoic Albany–Fraser Province. *J. Geol. Soc. Aust.* **30**, 333–340.

Foster, G., Kinny, P., Vance, D., Prince, C., Harris, N., 2000. The significance of monazite U-Th-Pb age data in metamorphic assemblages; a combined study of monazite and garnet chronometry. *Earth Planet. Sci. Lett.* **181**, 327–340.

Foster, G., Gibson, H.D., Parrish, R., Horstwood, M., Fraser, J., Tindle, A., 2002. Textural, chemical and isotopic insights into the nature and behaviour of metamorphic monazite. *Chem. Geol.* **191**, 183–207.

Gibson, H.D., Carr, S.D., Brown, R.L., Hamilton, M.A., 2004. Correlations between chemical and age domains in monazite, and metamorphic reactions involving major pelitic phases: integration of ID-TIMS and SHRIMP geochronology with Y–Th–U X-ray mapping. *Chem. Geol.* **211**, 237–260.

Giddings, J.W., 1976. Precambrian palaeomagnetism in Australia I: basic dykes and volcanics from the Yilgarn Block. *Tectonophysics* **30**, 91–108.

Harrison, T.M., Catlos, E.J., Montel, J.-M., 2002. U–Th–Pb dating of phosphate minerals. In: Kohn, M.J., Rakovan, J., Hughes, J.M. (Eds.). *Phosphates: Geochemical, Geobiological and Materials Importance*. Reviews in Mineralogy and Geochemistry, Vol. 48, Mineralogical Society of America, Washington, DC, USA, pp. 523–558.

Hawkins, D.P., Bowring, S.A., 1999. U–Pb monazite, xenotime and titanite geochronological constraints on the prograde to postpeak metamorphic thermal history of Paleoproterozoic migmatites from the Grand Canyon, Arizona. *Contrib. Mineral. Petrol.* **134**, 150–169.

Hollingsworth, D.A., 1996. Veining, metasomatism and metamorphism of metapelites of the Mount Barren Group at West Beach, Western Australia. BSc (Hons) thesis, Curtin Univ. Technology.

Kingsbury, J.A., Miller, C.F., Wooden, J.L., Harrison, T.M., 1993. Monazite paragenesis and U-Pb systematics in rocks of the eastern Mojave Desert, California, U.S.A.: implications for thermochronometry. *Chem. Geol.* **110**, 147–167.

Kohn, M.J., Malloy, M.A., 2004. Formation of monazite via prograde metamorphic reactions among common silicates: implications for age determinations. *Geochim. Cosmochim. Acta* **68**, 101–113.

Kohn, M.J., Wieland, M.S., Parkinson, C.D., Upreti, B.N., 2005. Five generations of monazite in Langtang gneisses: implications for chronology of the Himalayan metamorphic core. *J. Metamorphic Geol.* **23**, 399–406.

Kretz, R., 1983. Symbols for rock forming minerals. *Am. Mineral.* **68**, 277–279.

Lanzirotti, A., Hanson, G.N., 1996. Geochronology and geochemistry of multiple generations of monazite from the Wepawaug Schist, Connecticut, USA: implications for monazite stability in metamorphic rocks. *Contrib. Mineral. Petrol.* **125**, 332–340.

Montel, J.-M., Foret, S., Veschambre, M., Nicollet, C., Provost, A., 1996. Electron microprobe dating of monazite. *Chem. Geol.* **131**, 37–53.

Myers, J.S., 1990. Albany–Fraser Orogen. In *Geology and Mineral Resources of Western Australia*. Western Australia Geological Survey, Memoir 3, pp. 255–263.

Nelson, D.R., 1996. Compilation of SHRIMP U–Pb zircon geochronology data, 1995. Western Australia Geological Survey, Record 1996/5.

Nelson, D.R., 2001. An assessment of the determination of depositional ages for Precambrian clastic sedimentary rocks by U–Pb dating of detrital zircons. *Sediment. Geol.* **141–142**, 37–60.

Nelson, D.R., Myers, J.S., Nutman, A.P., 1995. Chronology and evolution of the middle Proterozoic Albany–Fraser orogen, Western Australia. *Aust. J. Earth Sci.* **42**, 481–495.

Overstreet, W.C., 1967. The geological occurrence of monazite. U.S. Geological Survey Professional Paper 530.

Parrish, R.R., 1990. U-Pb dating of monazite and its application to geological problems. *Can. J. Earth Sci.* **27**, 1431–1450.

Pisarevsky, S.A., Harris, L.B., 2001. Determination of magnetic anisotropy and a ca 1.2 Ga palaeomagnetic pole from the Bremer Bay area,

Albany Mobile Belt, Western Australia. *Aust. J. Earth Sci.* **48**, 101–112.

Pisarevsky, S.A., Wingate, M.T.D., Harris, L.B., 2003. Late Mesoproterozoic (ca 1.2 Ga) palaeomagnetism of the Albany–Fraser orogen: no pre-Rodinia Australia-Laurentia connection. *Geophys. J. Int.* **155**, F6–F11.

Post, N.J., Hensen, B.J., Kinny, P.D., 1997. Two metamorphic episodes during a 1340–1180 Ma convergent tectonic event in the Windmill Islands, East Antarctica. In: Ricci, C.A. (Ed.). *The Antarctic Region: Geological Evolution and Processes*. Terra Antarctica, Sienna, pp. 157–161.

Pyle, J.M., Spear, F.S., 2003. Four generations of accessory phase growth in low-pressure migmatites from SW New Hampshire. *Am. Mineral.* **88**, 338–351.

Rasmussen, B., Fletcher, I.R., 2004. Zirconolite: a new U–Pb chronometer for mafic igneous rocks. *Geology* **32**, 785–788.

Rasmussen, B., Bengtson, S., Fletcher, I.R., McNaughton, N.J., 2002. Discoidal impressions and trace-like fossils more than 1200 million years old. *Science* **296**, 1112–1115.

Rasmussen, B., Fletcher, I.R., McNaughton, N.J., 2001. Dating low-grade metamorphic events by SHRIMP U-Pb analysis of monazite in shales. *Geology* **29**, 963–966.

Rubatto, D., Williams, I.S., Buick, I.S., 2001. Zircon and monazite response to prograde metamorphism in the Reynolds Range, central Australia. *Contrib. Mineral. Petrol.* **140**, 458–468.

Sambridge, M.S., Compston, W., 1994. Mixture modelling of multi-component data sets with application to ion-probe zircon ages. *Earth Planet. Sci. Lett.* **128**, 373–390.

Sheraton, J.W., Tingey, R.J., Oliver, R.L., Black, L.P., 1995. Geology of the Bunger Hills-Denman Glacier region, East Antarctica. *AGSO Bull.*, 244.

Smith, H.A., Barreiro, B., 1990. Monazite U-Pb dating of staurolite grade metamorphism in pelitic schists. *Contrib. Mineral. Petrol.* **105**, 602–615.

Sofoulis, F.S., 1958. The geology of the Phillips River Goldfield, W.A. Western Australia Geological Survey, Bulletin, 110.

Spear, F.S., Pyle, J.M., 2002. Apatite, monazite, and xenotime in metamorphic rocks. In: Kohn, M.J., Rakovan, J., Hughes, J.M. (Eds.). *Phosphates: Geochemical, Geobiological and Materials Importance*. Reviews in Mineralogy and Geochemistry, Vol. 48, Mineralogical Society of America, Washington, DC, USA, pp. 293–335.

Stacey, J.S., Kramers, J.D., 1975. Approximation of terrestrial lead isotope evolution by a two-stage model. *Earth Planet. Sci. Lett.* **26**, 207–221.

Stephens, J.R., 1996. Structure and metamorphism of the east Mount Barren Area, Albany–Fraser Orogen, Western Australia. BSc (Hons) thesis, Curtin Univ. Technology.

Stern, R.A., Berman, R.G., 2000. Monazite U–Pb and Th–Pb geochronology by ion microprobe, with an application to in situ dating of an Archean metasedimentary rock. *Chem. Geol.* **172**, 113–130.

Tanaka, H., Idnurm, M., 1994. Palaeomagnetism of Proterozoic mafic intrusions and host rocks of the Mount Isa Inlier, Australia: revisited. *Precambrian Res.* **69**, 241–258.

Thom, R., 1977. The evolution of Proterozoic rocks near the Fraser Front at Ravensthorpe, Western Australia. PhD thesis, Imperial College.

Thom, R., Chin, R.J., 1984. Bremer Bay, W.A. Western Australia Geological Survey, 1:250000 Geological Series Explanatory Notes.

Thom, R., Lipple, S.L., Sanders, C.C., 1977. Ravensthorpe, W.A. Western Australia Geological Survey, 1:250000 Geological Series Explanatory Notes.

Thom, R., de Laeter, J.R., Libby, W.G., 1981. Rb–Sr dating of tectonic events in the Proterozoic Mount Barren Group near Hopetoun. Western Australia Geological Survey, Annual Report for 1980, pp. 109–112.

Vallini, D., Rasmussen, B., Krapez, B., Fletcher, I.R., McNaughton, N.J., 2002. Obtaining diagenetic ages from metamorphosed sedimentary rocks: U–Pb dating of unusually coarse xenotime cement in phosphatic sandstone. *Geology* **30**, 1083–1086.

Vallini, D., Rasmussen, B., Krapez, B., Fletcher, I.R., McNaughton, N.J., 2005. Microtextures, geochemistry and geochronology of authigenic xenotime: constraining the cementation history of a Palaeoproterozoic metasedimentary sequence. *Sedimentology* **52**, 101–122.

Wetherley, S., 1998. Tectonic evolution of the Mount Barren Group, Albany–Fraser Province, Western Australia. PhD thesis, Univ. Western Australia.

Wetherley, S., McNaughton, N.J., 1995. New age constraints on amphibolite facies mineral growth and deformation in metapelites: an example from the Mount Barren Group, Western Australia. *Proceedings of the Australian Conference on Geochronology and Isotope Geoscience, Workshop Program and Abstracts, Curtin University of Technology, Perth*, p. 38.

Wetherley, S., McNaughton, N., Kinny, P., 1998. Proterozoic tectonothermal events in the Albany-Fraser Province—how many, when and where? *Proceedings of the Tectonics Special Research Centre Inaugural Symposium, University of Western Australia, Perth, Abstracts*, pp. 82–86.

Williams, M.L., Jercinovic, M.J., 2002. Microprobe monazite geochronology: putting absolute time into microstructural analysis. *J. Struct. Geol.* **24**, 1013–1028.

Williams, M.L., Jercinovic, M.J., Terry, M.P., 1999. Age mapping and dating of monazite on the electron microprobe: deconvoluting multistage tectonic histories. *Geology* **27**, 1023–1026.

Wing, B.A., Ferry, J.M., Harrison, T.M., 2003. Prograde destruction and formation of monazite and allanite during contact and regional metamorphism of pelites: petrology and geochronology. *Contrib. Mineral. Petrol.* **145**, 228–250.

Wingate, M.T.D., Giddings, J.W., 2000. Age and paleomagnetism of the Mundine Well dyke swarm, Western Australia: implications for an Australia–Laurentia connection at 755 Ma. *Precambrian Res.* **100**, 335–357.

Wingate, M.T.D., Campbell, I.H., Harris, L.B., 2000. SHRIMP baddeleyite age for the Fraser dyke swarm, southeast Yilgarn Craton, Western Australia. *Aust. J. Earth Sci.* **47**, 309–313.

Wingate, M.T.D., Morris, P.A., Pirajno, F., Pidgeon, R.T., 2005. Two Large igneous provinces in late Mesoproterozoic Australia. *Geol. Soc. Aust. Abst.* **81**, 151.

Wingate, M.T.D., Pisarevsky, S.A., Evans, D.A.D., 2002. Rodinia connections between Australia and Laurentia: no SWEAT, no AUSWUS? *Terra Nova* **14**, 121–128.

Witt, W.K., 1997. Geology of the Ravensthorpe and Cocanarup 1:100 000 sheets. Western Australia Geological Survey, 1:100000 Geological Series Explanatory Notes.

Witt, W.K., 1998. Geology and Mineral Resources of the Ravensthorpe and Cocanarup 1:100000 Sheets. Western Australia Geological Survey, Report 54, Perth, 152 p.

Zhu, X.K., O'Nions, R.K., 1999. Monazite chemical composition: some implications for monazite geochronology. *Contrib. Mineral. Petrol.* **137**, 351–363.